ASSESSING THE IMPACTS OF LAND MANAGEMENT PRACTICES ON SURFACE RUNOFF AND SOIL EROSION IN NAM-CHUN WATERSHED, NORTHERN THAILAND

AKPEJIORI, ILAMOSI JULIET
February, 2018

SUPERVISORS:
Dr. D. B. P. Shrestha
Dr. D. Alkema

ASSESSING THE IMPACTS OF LAND MANAGEMENT PRACTICES ON SURFACE RUNOFF AND SOIL EROSION IN NAM-CHUN WATERSHED, NORTHERN THAILAND

AKPEJIORI, ILAMOSI JULIET
Enschede, The Netherlands,
February, 2018

Thesis submitted to the Faculty of Geo-Information Science and Earth Observation of the University of Twente in partial fulfilment of the requirements for the degree of Master of Science in Geo-Information Science and Earth Observation.
Specialization: Applied Earth Sciences with specialization in Natural Hazards, Risk and Engineering

SUPERVISORS:
Dr. D. B. P. Shrestha
Dr. D. Alkema

THESIS ASSESSMENT BOARD:
Prof. N. Kerle (Chair)
Dr. T.A. Bogaard (External Examiner, TUDelft)

ABSTRACT

Excessive surface runoff after massive rainfall influences flooding at the downstream side of a watershed and erosion problems in the upstream parts. The generation of excessive runoff, which is the source of these problems, can be attributed to land modification practices such as deforestation and intensive agricultural practices thereby reducing the underlying soil's ability to retain more water by infiltration. In this research, rainfall-runoff modelling was carried out with the use of the physically-distributed model, Limburg soil and erosion model (LISEM) to simulate scenarios of increment in rainfall intensity, land cover changes, vegetation changes and land management effects in the Nam-Chun watershed, situated in Phetchabun province, North-central Thailand.

LISEM was used to simulate the influence of different factors on runoff generation and soil loss. Soil, topographical and land cover properties such as saturated hydraulic conductivity, random roughness and Manning's n were adjusted to incorporate the effects of land management in the model. As part of the research, a method of estimating vegetation cover percentage by combining field assessment and satellite imagery with Random Forests regression was used. The effect of seasonal vegetation changes and long-term land cover change (from 2000 to 2017) on changing the runoff and soil loss characteristics of a catchment were also simulated. The effect of changing different rainfall storms on increasing runoff discharge was simulated. Land management practices were modelled by adjusting the LISEM model input parameters.

Analysis of the results shows that long-term land cover changes influenced the runoff discharge and soil loss in the watershed. Reduction in the percentage of vegetation cover also reduces the ability of plants to intercept rainfall and reduce soil detachment by the rainfall impact. Increase in rainfall intensity results in increased runoff discharge and soil loss rates. Implementation of reforestation, terracing and mulching reduced the runoff discharge and soil loss between 10-30% for the whole catchment. Reforestation measures were observed to reduce runoff and soil loss in a watershed efficiently.

Keywords: remote sensing, vegetation cover, rainfall-runoff modelling, land management, watershed,

ACKNOWLEDGEMENTS

I would like to express my gratitude to the Faculty of Geo-Information Science and Earth observation for granting me the scholarship to undertake this Master of Science degree course in the Netherlands. I also like to thank my employer, University of Benin, Benin City, Nigeria for granting me study leave.

Special thanks to my supervisors, Dr Dhruba Shrestha and Dr Dinand Alkema for their guidance throughout this research work. Their advice and criticisms were immensely useful in the course of this thesis work. Encouragements from them eased much pressure.

All the staff of the Earth Systems analysis department have helped in achieving this MSc degree including Prof Victor Jetten whose great advice helped me in the course of the MSc research phase, Dr Janneke. Ettema and Dr Nanette C. Kingma for their motherly advice in times of research difficulty, Prof. Norman Kerle, Ir. Bart Krol, Dr Olga Mavrouli, Dr Cees van Westen, Bastian van den Bout who provided help while setting up the LISEM model and all others.

My heartfelt appreciation goes to the institutions which provided research support for this project including National Aeronautics and Space Administration (NASA), Asian Disaster Preparedness Centre (ADPC) Bangkok, Naresuan University Phitsanulok and the SERVIR-Mekong team in ADPC where I did an internship for the development of this thesis. Dr Ate Poortinga and Dr Nguyen Hanh Quyen are especially recognised for all their assistance during my stay at ADPC.

I especially thank Prof. Jacob Ehiorobo for his fatherly guidance and support to achieve this degree. Special recognition goes to my family for their support. To my mother, Mrs Clara Akpejiori, thank you for all the sacrifices you made to see me have a good education. To my brother Ethasor Akpejiori and sister Mrs Okhiaofe Ameh, thank you for believing in me.

The support from friends I made here in Enschede has kept me going in the face of difficulty these last 18 months. Jefferson, Agbor, Belinda and Musa thanks for not making me miss home too much. To all my AES classmates, thank you all for the support. I especially recognise my best friend and confidant, Ighodalo Ahuean. Your encouragement in achieving this degree will never be forgotten.

I dedicate this thesis to God, with whom I live, move and have my being.

TABLE OF CONTENTS

LIST OF FIGURES

LIST OF TABLES

1. INTRODUCTION

1.1. Background

In recent times, many parts of the world have experienced worst cases of hydro-meteorological disasters. Many places have been experiencing heavy rainfall storms and typhoons which have led to the loss of lives and damage to property. According to the EM-DAT database on disasters (accessed at http://www.emdat.be/publications), hydrological disasters in 2016 were the most significant cause of property damage by natural disasters in the world (Guha-Sapir et al., 2016). According to Guha-Sapir et al. (2016), Asia is the most affected continent by hydrological disasters, with India and China being the worst hit countries by heavy rainfall and floods. Flooding has been a recurring problem leading to billions of dollars in losses almost every year since 2000. Southeast Asia has experienced a long history of flooding events and resulting damage to property and loss of lives. In many regions of Thailand, one of the largest economies in Southeast Asia, flood events have been recurrent. The tropical monsoonal rainfall characterising the area has been observed to be on an increasing trend over the years (Piman et al., 2016). In 2001, significant parts of Thailand battled flooding due to Typhon Usagi causing massive damage to property. The floods of July 2011 from Storm Haima (Nock-ten) were said to be the worst flooding in fifty years (Bidorn et al., 2015). The damages due that 2011 singular flood event in Thailand was over 42 billion dollars (Guha-Sapir et al., 2016).

The problem of flooding is primarily due to excess runoff over the land surface. Excessive surface runoff usually forms as a result of the soil's inability to hold stormwater during a rainfall event (García-Ruiz et al., 2010). It originates from hillslopes during or after rainfall events, when either surface depression storage, soil moisture or infiltration capacity is exceeded (Morgan, 2005). When surface runoff becomes too much for channels to handle, it can result in floods. The upstream areas contributing to floodplains are not excluded from the effects of excessive runoff as high-velocity runoff along slopes carries off sediments along its path. As this progresses, gully formation occurs and becomes a challenge most farmers in those areas have to combat. Excessive surface runoff is a problem for areas with high slopes as erosion by water becomes inevitable especially when soil conservation measures are absent. During periods of high rainfall, damages occur as a result of excessive runoff leading to flash flooding and erosion. The severity of runoff-related hazards in a catchment basin depends on the rainfall, vegetation cover, soil properties, topography, and land use practices (Cuomo et al., 2015). In agrarian watersheds, soil loss and runoff are mostly generated in farmlands, more than any other land use types (Wang et al., 2017). In some areas, agriculture is practised on steep slopes where minimal conservation measures are in place except for the farmers leaving behind residues of harvested crops which help to protect the soil by resistance to raindrop impact.

Although soil and water conservation efforts are implemented by reforestation programs and building of dams and reservoirs in some parts of Thailand, there is need to assess the effectiveness of these measures in the reduction of surface runoff and sediment discharge as climatic influences have changed through the years. Since the climate is becoming more dynamic especially for tropical regions (Artlert et al., 2013), there is a need for studies on how to prevent future occurrences of flash floods for the downstream areas. Watershed restoration can be done by implementing conservation measures, the effect of which can be simulated using hydrological models. Conservation measures have been studied in regards to runoff modelling. Palese et al. (2015) estimated the influence of management practices such as grass coverage and tilling of the soil on runoff and sediment yield in olives groves on sloping lands in Southern Italy. It was concluded in the research that in olive micro-plots with 100% ground vegetation cover, the ground cover had sufficiently reduced surface runoff and sediment when compared with olive micro-plots which were had lesser ground cover and tilled. The impact of land cover changes and runoff control management have also been analysed for the Mediterranean region of southern France (Fox et al., 2012). In this study, it was shown that land cover changes are the primary drivers of the increase in runoff even when engineering control measures are in place in flood-prone areas. It is, therefore, necessary that a combination of structural control measures together with providing more green spaces can efficiently reduce flooding and erosion. Studies on the effectiveness of runoff and soil loss control measures for south-eastern Asian tropical catchments is however limited.

1.2. Problem description

1.2.1. Factors influencing flash flooding and erosion

The primary cause of the problem of flash flooding and erosion is severe deforestation which has occurred over the years due to the need to create adequate land for agriculture. Farming on the hillslopes is also practised in many areas (Shrestha et al., 2014). The soils are tilled and ploughed excessively, losing their natural structure which can result in adverse effects of excessive runoff and soil loss. Studies have been carried out to assess erosion and flooding, but there is a need for further studies on best practices which can curb the recurrent erosion and flooding generated by excessive runoff from slopes. This study will look into methods in which excessive flow can be controlled by adjusting the land management practices and implementing soil and water conservation measures in the study area.

Vegetation cover is an essential factor to consider in land degradation studies as it determines the resistance to rainfall impact and overland flow to erosion and flooding. It is used to derive canopy cover fraction, leaf area index (LAI), interception, throughfall and other hydrological elements required in rainfall-runoff modelling. It is an essential factor in water and soil conservation analysis (Jia et al., 2016; Niu et al., 2014). Remote sensing techniques are used to derive vegetation indices which can be used as a proxy to estimate vegetation cover present in the catchment. An example of such indices is the Normalized Difference

Vegetation Index (NDVI) which is used to derive canopy cover fraction as input to modelling interception for the areas under study (Jensen, 2007; Shrestha et al., 2014).

However, vegetation cover derived from vegetation indices such as NDVI is not usually representative of the actual state of vegetation in the area (Van der Knijff et al., 1999). The effect of base vegetation such as litter and shrubs under canopy trees is usually neglected. There is a need for studies to determine the amount of surface runoff that is obstructed due to the presence of shrubs underneath tree canopies (Hadi et al., 2016). LiDAR data has been used for cover validation, but it is advised that field data be used to reduce errors due to LiDAR sensor imperfections such as scanning geometry (Korhonen et al., 2013). LiDAR data is also quite expensive to obtain for monitoring of large areas.

Rainfall characteristics of the region to be studied is also crucial in hydrological modelling. Cuomo et al., (2015) used LISEM to model the effects of different rainfall scenarios to determine the runoff and sediment yield estimates for unsaturated soils. He concluded that the characteristics of runoff depend on the rainfall hyetograph of the area and that rainfall scenario studies are necessary when assessing the hydrological properties of a catchment.

1.2.2. Rainfall-runoff modelling

One of the primary divisions in rainfall-runoff models are lumped or distributed models (Beven, 2012). Lumped models treat the catchment as a unit, giving average outputs over the area. Distributed models require every parameter specified in each element in the whole area. The lumped models may require fewer input data to run. An example of a lumped rainfall-runoff model which also serves as a soil loss assessment model is the Universal Soil Loss Equation (USLE). Distributed models are more detailed as processes incorporate spatial attributes which make them a useful tool for prediction. Examples of distributed models are MIKE Systeme Hydrologique Européen (MIKE-SHE) model, Topography-based hydrological model (TOPMODEL), European Soil Erosion Model (EUROSEM), Areal Nonpoint Source Watershed Environment Response Simulation (ANSWERS), Agricultural Non-Point Source pollution model (AGNPS), Soil and Water Assessment Tool (SWAT), and Limburg Soil Erosion Model (LISEM).

Several distributed models also known as physically-based models can be used to assess runoff and soil loss patterns in a watershed at user-defined levels. Some of them are annual-based, daily or event-based models. Annual models such as the Universal Soil Loss Equation (USLE) give generalised results about a catchment while daily, hourly or event-based models such as the Limburg Soil and Water Erosion Model (LISEM) can give more detailed results depending on the spatial level at which the user wishes to interpret the output results (Hölzel & Diekkrüger, 2012). Most lumped annual models such as USLE require fewer input parameters and more responsive to scenarios with fewer data requirements (Blanco-Canqui & Lal, 2010).

Lumped and distributed models may also have different outputs when compared with each other because each model has its peculiar capability (Bazrkar et al., 2017).

When using physically based models like OpenLISEM, physical parameters such as vegetation cover, the soil conductivity, and initial soil moisture conditions have to be used as input for the various processes of the rainfall-runoff cycle (Beven, 2012). Since vegetation is a crucial factor in runoff behaviour, field measurements of cover percentages per unit land use will be a way of deriving calibration data for such models. Studies on the effect of vegetative cover for degradation studies have mainly focused on aspects of soil loss for upstream river catchments (Ouyang et al., 2010; Zhou et al., 2008). Since surface runoff is the primary driver of soil loss, there is a need for studies on land cover management for reduction of surface runoff. Field measurements can be carried out to assess vegetation at locations and the resulting data used to estimate for the whole area by using statistical methods.

1.3. Objectives and research questions

The general objective is to analyse the impact of different conservation measures and land management practices on surface runoff and soil loss in Nam-Chun watershed, Northern Thailand. The specific objectives and research questions following them are as follows:

1. Estimating land cover parameters for surface runoff and soil loss
    a) What is the relationship between NDVI and vegetation cover for different land cover types in tropical areas?
    b) What method can be used to upscale land cover information for the whole watershed?
2. Evaluating the mechanism of hydrological processes of surface runoff and soil loss
    a) Which hydrological elements are influenced by vegetation variation?
    b) Which input model parameters more sensitive in assessing runoff and effects of conservation?
    c) What is the amount of runoff generated for different rainfall storms?
3. Analysis of the land management effects in response to rainfall intensity and duration scenarios
    a) Which land management practices are more suitable for the current rainfall pattern in Thailand?
    b) What is the present state of conservation in the watershed?
    c) Which areas and under which rainstorms are susceptible to erosion?
    d) What is the effect of increasing rainfall magnitudes on soil and water conservation measures for a tropical catchment?

1.4. Thesis structure

Chapter one describes the introduction, the basis and objectives of the research carried out. Chapter two details the study area description, data and methods to achieve the set objectives. Chapter three shows the results from the methodological approach in achieving the set objectives. Chapter four shows further results and analysis of the scenarios developed. Chapter five discusses the outcome of the results and their relevance in answering the research questions. Chapter six concludes the thesis, showing the limitations and proffers recommendations in improving the research.

2. METHODOLOGY

While setting out to carry out the objectives listed in chapter one, the following methodology was adopted as illustrated in the flowchart in Figure 2.1. The chosen approach is divided into three broad aspects: land cover change analysis, rainfall distribution analysis, and modelling rainfall-runoff and erosion scenarios. The study area is also described below.

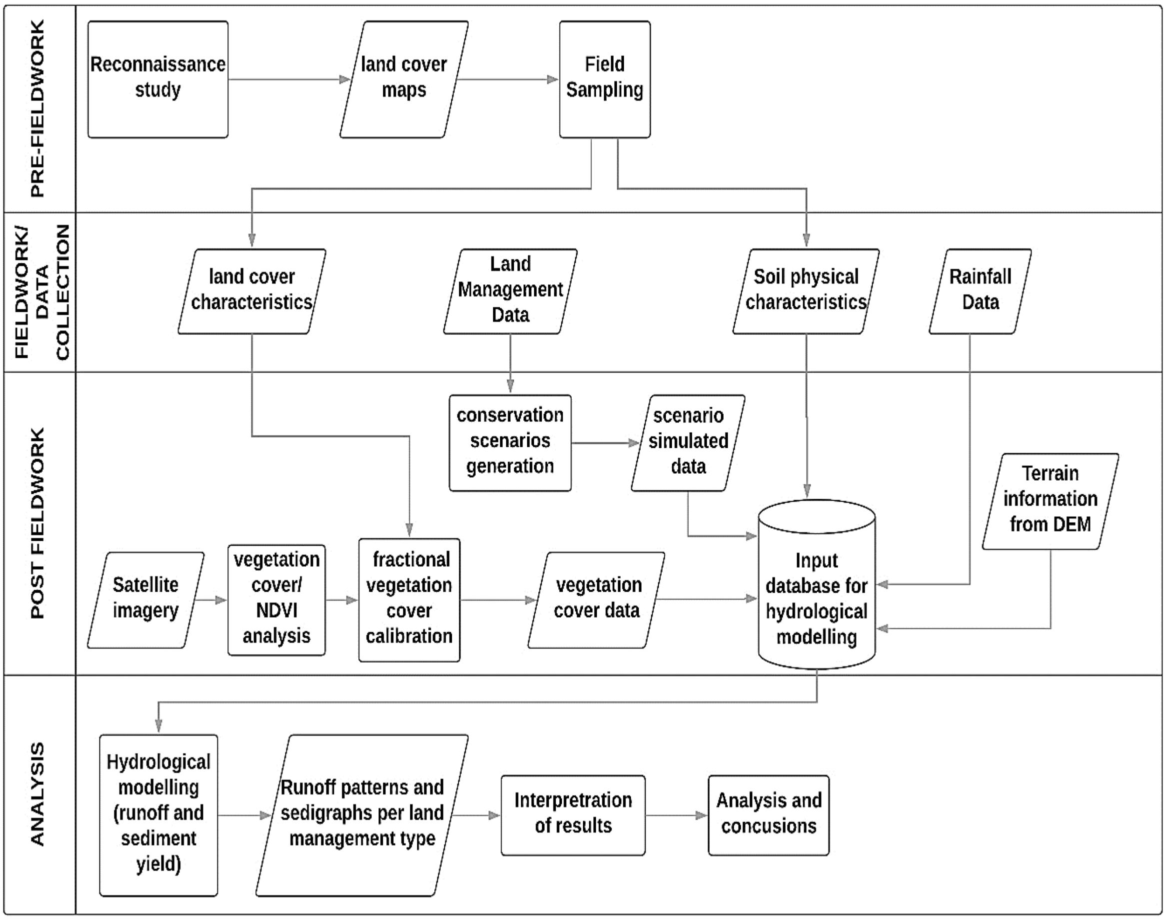

Figure 2.1 Methodology flow chart

2.1. Study area

Nam-Chun watershed is a mountainous tropical catchment located in Lomsak district in Phetchabun province, North-Central Thailand. It is bounded by latitudes 16˚40′and 16˚50′north and longitudes 101˚02" and 101˚15" east. It covers a total area of about 72.5 square kilometres. The elevation varies from 180–1490 meters above sea level and is characterized by steep slopes and narrow valleys. Two mountain rivers drain to become the Nam Chun river which has a history of flooding to the lowland regions. Daily rainfall can be as high as 132 mm, with the region experiencing an average annual rainfall of about 1087mm. The rainy season lasts from May until October with occasional monsoons. Rain-fed annual cropping of crops such as maize, beans, cabbage and vegetables is majorly practiced in the agricultural area. Tamarind orchards and teak plantations are also abundant.

The conservation measures adopted are the protection of forest areas, reforestation of degraded forest areas, and forbidding farmers to cultivate on steep slopes. In 2013, a dam was also built in the middle of the watershed to control flooding downstream. Some farmers practice shifting cultivation, mixed farming, and burning of forest to create arable land, a method known as 'slash and burn'. Studies on soil loss and runoff assessment have concluded that agricultural areas need to be better managed to prevent flash flood and erosion (Shrestha et al., 2014).

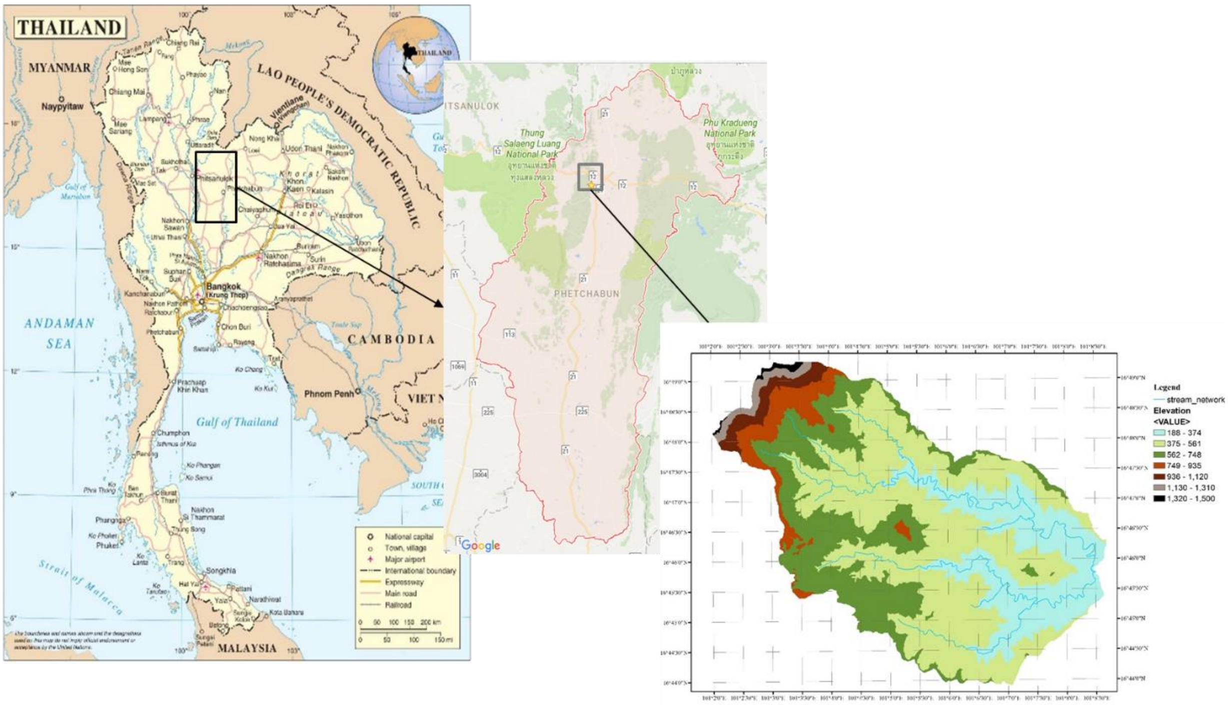

Figure 2.2 Study area

2.2. Data collection

Data required for this study had to be collected from the field and offices. They are summarised in Table 2.1.

Table 2.1 Data collected for the study

DATA	Description	Availability/Source
Optical imagery	Multispectral imagery (Sentinel-2 and Landsat). Processed with Google Earth Engine	Copernicus and NASA
Rainfall data	High temporal and Long-term data	Royal Meteorological Department, Thailand
DEM	High resolution (5m)	Land development department Thailand
Land cover maps	Annual maps of the region	previous studies and available online from SERVIR-Mekong/ADPC
Soil samples	For derivation of Soil physical characteristics: soil saturated water content, soil bulk density, soil porosity, soil organic matter content and saturated hydraulic conductivity	Field measurements and subsequent laboratory analysis in Naresuan University
Land management information	Information on agricultural practices	Field verification and information from Land development department

2.2.1. Fieldwork

Fieldwork in the Namchun watershed area lasted for ten days starting from the 14th of September to the 24th of September 2017. Data on vegetation cover and NDVI were collected from 84 locations. Undisturbed samples of soil were collected from 16 locations for further analysis of soil properties in the laboratory. Undisturbed sampled were collected to obtain an indication of the in-situ saturated conductivity while maintaining the soil structure at the sample location.

2.2.2. Soil sampling

Undisturbed soil samples were collected from sixteen locations from some forest, agricultural, grasslands and bare fields. Soil sampling was done at a depth of 5cm below the surface with a steel core sampler of 5 cm diameter and 5 cm height. They were then sealed and taken to the laboratory for saturated hydraulic conductivity tests and bulk density measurements.

Figure 2.3 Undisturbed soil sampling in the field

2.2.3. Laboratory analysis

The laboratory testing started on the 27th of September to the 2nd of October 2017 at the Civil engineering laboratory of the Naresuan University in Phitsanulok, Thailand. The undisturbed samples were analysed for the saturated hydraulic conductivity, bulk density, moisture content, texture analysis and porosity. As a suitable apparatus was not available for measuring saturated hydraulic conductivity for undisturbed samples, an apparatus was constructed to do the test as shown in Figure 2.4. The samples were first soaked for a day. The amount of water passing through each sample was measured at one-minute interval while keeping the level of water above it constant. Values were recorded between 3 to 4 hours, depending on when the readings became constant for each soil sample. The samples were then measured after the Saturated hydraulic test was conducted, oven-dried for 24 hours and after that weighed to compute the bulk density, particle density and porosity of each soil sample according to Equations 2.1, 2.2 and 2.3.

Figure 2.4 Saturated hydraulic conductivity apparatus

$$Bulk\ density\ (g/cm^3) = \frac{weight\ of\ dry\ soil}{volume\ of\ container} \ldots\ldots 2.1$$

$$Particle\ density (g/cm^3) = \frac{weightof\ dry\ soil}{volume\ of\ soil\ particles} \ldots\ldots 2.2$$

$$Porosity\ (\%) = 100 - \left(\frac{bulk\ density}{particle\ density} X\ 100\right) \ldots\ldots 2.3$$

2.3. Vegetation cover estimation

Eighty-four locations were randomly-sampled for the percentage coverage of bare soil, litter, shrubs and tree canopy cover in a 10-m square grid (Figure 2.6). The estimates were done using a standard chart (Figure 2.7) published by California Native Plant Society (CNPS) for cover estimation (CNPS, n.d.). The canopy cover was measured using a spherical densiometer, adopting the procedure according to Gqd (n.d.). The NDVI measurements for each component of vegetation (bare soil, shrubs, canopy) at all locations were taken with a handheld Green Seeker handheld crop sensor shown in Figure 2.5. The weighted-average NDVI for each area was obtained by multiplying the NDVI measured for each vegetation component (bare soil, shrubs, canopy) by the component cover percentage as shown in Equation 2.4.

$$Weighted\ field\ NDVI\ for\ each\ location\ = \frac{NDVI_{tree} + NDVI_{shrub}\ + NDVI_{soil}}{\%_{tree} + \%_{shrub} + \%_{soil}} \ldots\ldots 2.4$$

Figure 2.5 Equipment for field NDVI measurement

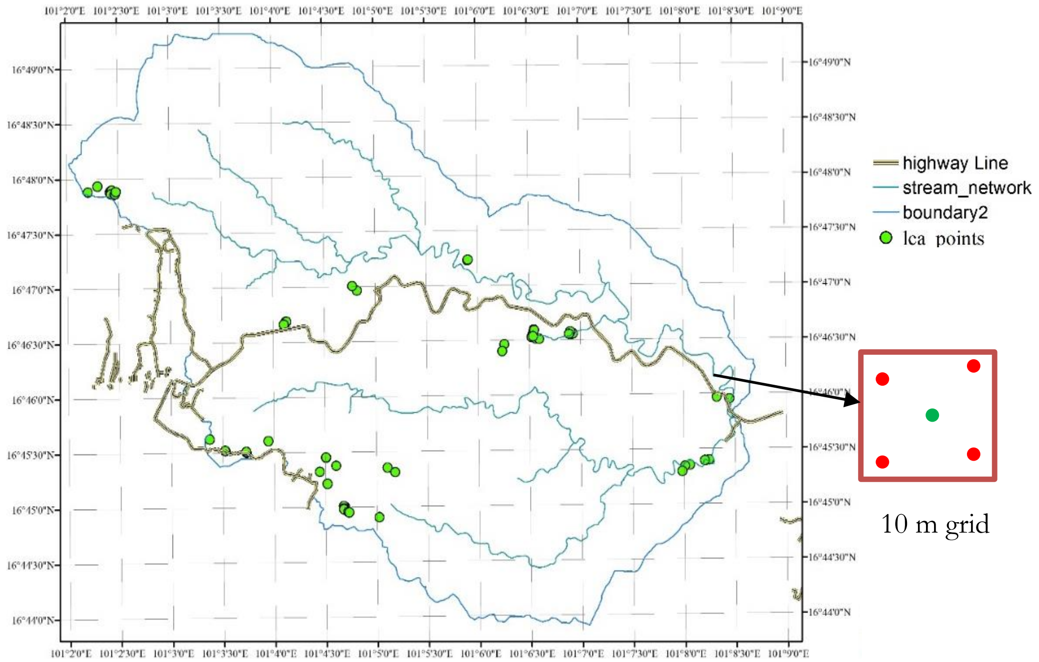

Figure 2.6 Map of the locations were vegetation cover assessment was carried out during fieldwork.

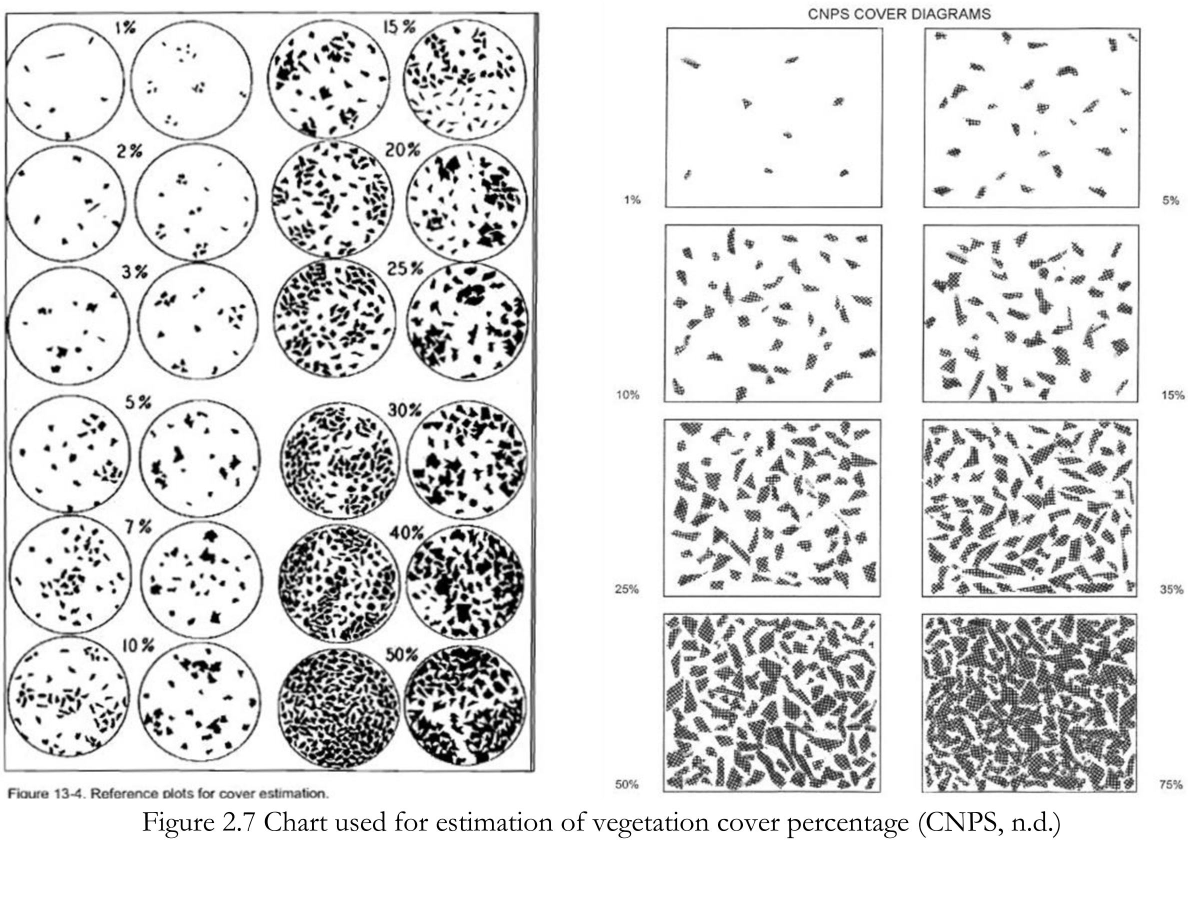

Figure 2.7 Chart used for estimation of vegetation cover percentage (CNPS, n.d.)

2.3.1. Image processing

Satellite images used for both land cover classification and vegetation cover estimation were processed with a recently-developed coding interface developed by Google®, Google Earth Engine, for faster processing of remote sensing products(United States Department of Agriculture, n.d.). It allows for large-scale satellite data to be processed on a cloud server without having to download massive data and use up large computer memory. The processed results required can be downloaded within the boundaries of the study area. Using the interface helps to minimise computer memory usage and processing power since there is no need to download a significant amount of satellite data. User-specific data can also be uploaded and used for analysis on the cloud servers.

For the study, Sentinel-2 and Landsat-7 imagery were used for estimating vegetation cover for the dry and wet seasons in 2000 and 2017. Sentinel- 2 imagery with a spatial resolution of 10 meters was available for 2017 (dry season in 7th April 2017 and the wet season also coincident with the fieldwork period on 14th September 2017). Landsat-7 imagery with a spatial resolution of 30 meters was used for images of 2000 (dry season in 7th of March 2000 and the wet season in 2nd of November 2000). The false-colour composite images are shown in Figure 2.9. Cloud presence was removed by masking out the cloud pixels using cloud removal algorithms which use the cloud and cirrus bands in the imagery. The algorithm was available on the Google earth engine repository ('Google Earth Engine', n.d.). Some areas were left empty after cloud masking. To get values for the masked out pixels, they were filled with cloud-free pixels from images of 29th September 2016, 9th September 2017, 4th October 2017,19th October 2017 and 24th October 2017 (all images from the wet season). The resulting composite image had 95% of the pixels from the satellite image of 14th September 2017. Although the image was clear, patches of cloud were still present. Errors as a result of these patches of clouds were removed by applying conditional statements in PCRaster to remove the false values of vegetation cover for specific land cover types.

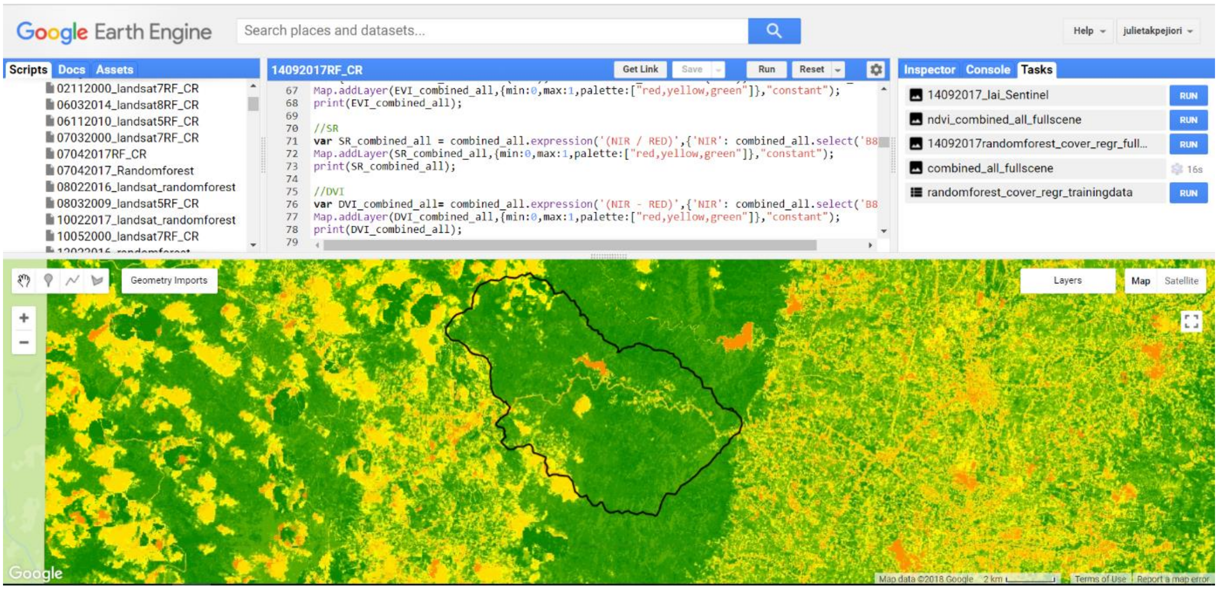

Figure 2.8 Image processing with Google earth engine interface

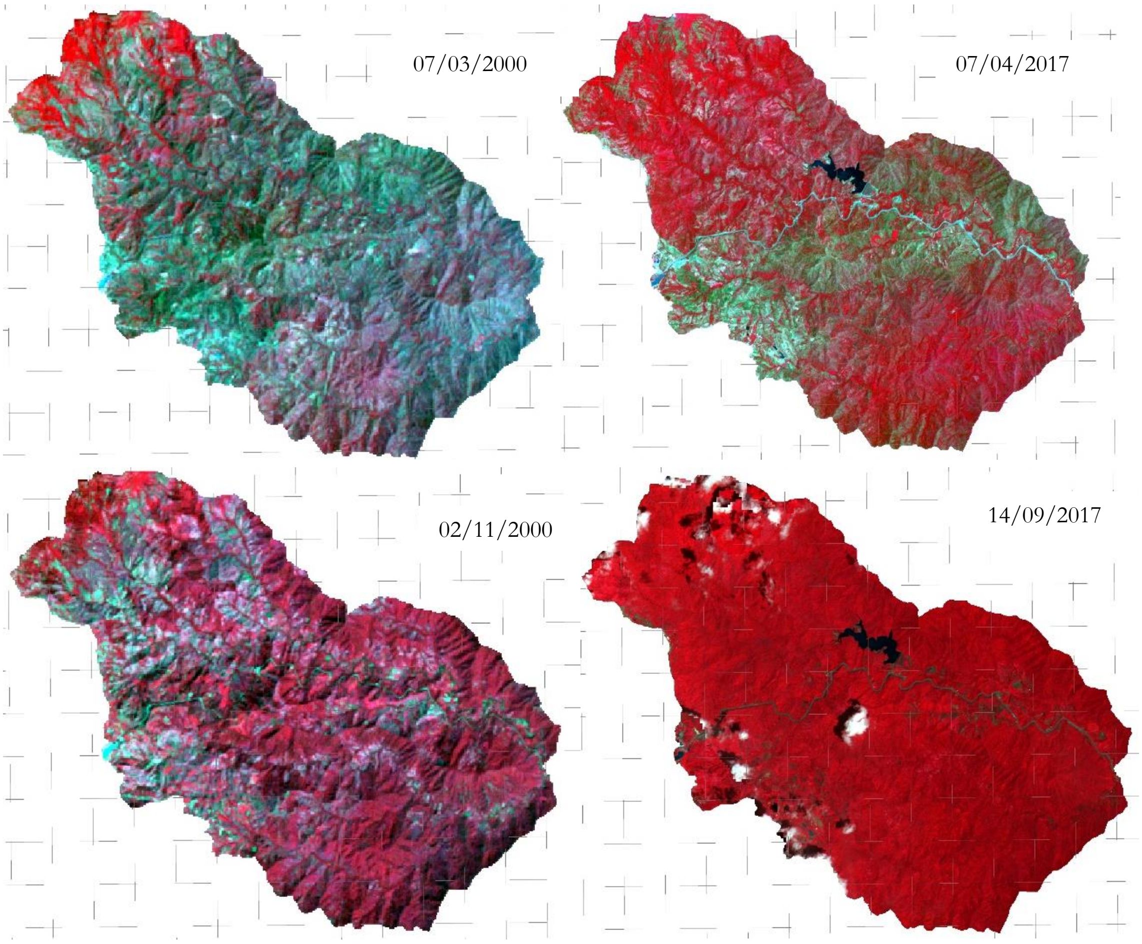

Figure 2.9 False colour composite of the imagery from the selected dates

2.3.2. Vegetation cover estimation with Random forest regression

Vegetation cover percentage is an essential variable for runoff modelling as an input for interception estimation (de Jong & Jetten, 2007; Li, Wang, & Li, 2015; Jia et al., 2016). Proxies such as Normalized Difference Vegetation Index (NDVI) are sometimes used to estimate percentage vegetation cover from satellite images (Van der Knijff et al., 1999). Vegetation cover estimation is an essential aspect of hydrological modelling and is to estimate the amount of rainfall which is intercepted by trees which is essential for the calculating general water balance. Usually, the values of NDVI derived from a satellite image are assumed to be an indication of vegetation cover in the area which may not be the case as it is an over-simplification for the model and does not resemble the reality on the ground. Several studies have been carried out to address this problem (Jia et al., 2016; Zhou et al., 2008). Field vegetation cover estimation would be a more accurate way to determine percentage vegetation cover. Percentage vegetation cover is estimated in the area on field plot scales. It is usually a challenge to derive vegetation cover for the whole area by this method. Some researchers have used machine learning techniques such as support vector machines (SVM), non-parametric nearest neighbour (KNN) regression and random forest (RF) regression for prediction to derive vegetation cover and other ecological parameters with remote sensing variables (Peters et al., 2007; Zhou et al., 2008; Grinand et al., 2013; Zafari et al., 2017). Each of this techniques differs in capability for different applications depending on the image spatial resolution and number of field plots measured.

Random forest regression is a machine learning technique which can be used as classification technique. It produces decision trees using a random subset of training variables which can be used to classify an image based on measurements and associated parameters (Belgiu & Drăgut, 2016; Peters et al., 2007). Random Forest regression is a more applicable tool in the case of fewer training sample sizes. Being a non-parametric classifier, it does not assume frequency distributions and is suitable for implementing remote sensing variables which do not usually have normal distributions (Belgiu & Drăgut, 2016). Prediction is performed on the image based a target parameter (vegetation cover) by creating classification and regression trees (Breiman, 2001). It is a means of classification involving a probabilistic scheme to assign significance to the various input variables.

In this study, satellite image pixel radiometric resolution (red, green and near infra-red bands) and vegetation indices were used as parameters to predict vegetation cover for the whole watershed for hydrological modelling. Percentage vegetation cover estimates obtained from the field were used to classify satellite images by using the Random Forest (RF) regression which was used to estimate values based on field observations from section 2.3. Based on the 84 vegetation cover estimates from the field, a vegetation prediction was carried for the whole area. The vegetation cover percentages that were obtained this way for the entire watershed were used in the hydrological model, LISEM. Satellite image spectral values and vegetation indices relating to vegetation cover were used to classify an image obtained during the fieldwork period (14th of September, 2017) to estimate vegetation cover. The prediction was based on the relationship created by Random Forest Regression between the pixel bands. The red, green, red edge and near infra-red bands were selected based on their importance in indicating vegetation presence using remote sensing. The vegetation indices considered were Simple Ratio (SR), Enhanced Vegetation Index (EVI), Normalized Difference Vegetation Index (NDVI), and Difference Vegetation index (DVI) which are quite sensitive to vegetation cover (Barati et al., 2011). These were used to predict the adjusted vegetation cover values obtained by using the relationship between NDVI measured in the field and vegetation cover estimated at the 84 locations within the study area.

2.4. Land cover classification

Land cover maps from the years 2000 to 2017 were obtained from the Regional land cover monitoring system (RLCMS) database (available on http://servir-rlcms.appspot.com/static/html/map.html) developed by SERVIR-Mekong, a research unit under the Asian Disaster Preparedness Centre in Bangkok. The land cover maps have been produced for the Southeast Asian countries in the Mekong river basin to cater for the needs of government authorities in the region to have a uniform planning and decision-making tool.

The land cover classification methodology is shown in a flowchart in Figure 2.10. Field verification data regarding percentage canopy cover, tree height, percentage shrub cover and other variables collected in various locations within the Mekong region were used to create the annual land cover maps. The land cover maps were created using classification algorithms. A classification algorithm is used to classify the image using a mixture of various remote sensing derivatives and thematic primitives (such as the percentage of canopy cover, forest types, the percentage of water, and others shown in Figure 2.11). These primitives form the basis for all class probabilities. The probabilities are defined from a Monte Carlo simulation with a mixture of different spectral band combinations in the form of spectral indices. Land cover classes, such as deciduous forest, cropland, urban areas and so on, are derived from a defined probability decision tree shown in Figure 2.13. For accuracy assessment shown in Figure 2.12, a confusion matrix is created with the reference data and the classifications from the imagery. A decision tree helps in using the results in assigning the appropriate land cover class to each satellite image pixel. The decision tree is also applied to images of previous periods using the same training data model to obtain land cover images from other time periods (SERVIR-Mekong, 2017; SERVIR, n.d.).

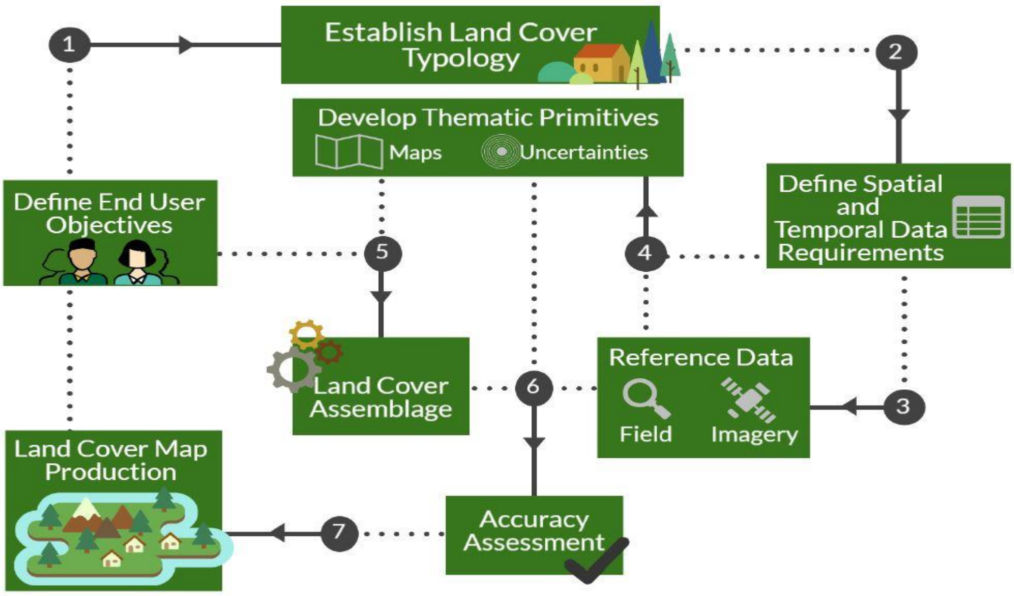

Figure 2.10 Methodology of land cover classification in the RLCMS (SERVIR-Mekong, 2016)

Group	Primitives: End Component (Thematic)	Primitives: Biophysical (Continuous & Thematic)
Forest	Bamboo	% Tree Canopy cover
	Mangrove	Tree height
		Forest Cover (MMU)
		Phenology (deciduous/evergreen)
		Broadleaf vs needleleaf
Agriculture	Cropland	Shifting cultivation
	Plantation - Crop (rubber, oil palm)	
	Plantation-Forest	
	Rice Paddy	
Settlement	Urban	% Impervious surface
Water, Wetland, Snow/Ice	Snow/Ice	% Inundation
	Ephemeral Water	
Grassland, Bare Land, Shrubland	Mining (Bare Land)	% Shrub cover
	Mud Flats (Bare Land)	% Grass cover
	Barren (Bare Land)	

Setting	Origin	Life Form	Class	Class Description
Terrestrial	Natural / Semi-Natural	Forest	Deciduous Forest	Lands dominated by trees (>=10% tree canopy cover), where majority of tree cover represented by trees >5m in height. Deciduous tree species make up >60% of the total tree cover.
Terrestrial	Natural / Semi-Natural	Forest	Evergreen Broadleaf Forest (not subalpine)	Lands dominated by trees (>=10% tree canopy cover), where majority of tree cover represented by trees >5m in height. Evergreen broadleaf tree species make up >60% of the total tree cover.
Terrestrial	Natural / Semi-Natural	Forest	Evergreen Broadleaf Forest - Subalpine	Lands dominated by trees (>= 10% tree canopy cover), where majority of tree cover represented by trees >2m in height. Rhododendron tree species make up >60% of the total tree cover.
Terrestrial	Natural / Semi-Natural	Forest	Evergreen Needleleaf Forest	Lands dominated by trees (>=10% tree canopy cover), where majority of tree cover represented by trees >5m in height. Evergreen needleleaf tree species make up >60% of the total tree cover.
Terrestrial	Natural / Semi-Natural	Forest	Mixed Forest	Lands dominated by trees (>= 10% canopy cover), where majority of tree cover represented by trees >5m in height. Represented by mixture of forest cover types where no single cover type makes up >60% of the total tree cover.
Terrestrial	Natural / Semi-Natural	Forest	Bamboo	Lands dominated by trees and bamboo (>= 10% tree canopy cover), where majority of tree cover represented by trees >5m in height. Bamboo make up >60% of the total tree and bamboo canopy cover.
Terrestrial	Natural / Semi-Natural	Non-Forerst	Barren	Natural/semi-natural lands with majority aerial extent comprised of exposed soil, sand, rocks.
Terrestrial	Natural / Semi-Natural	Non-Forerst	Grassland/ Herbland	Lands with herbaceous cover, where wetland obligate species are scarce. The aerial extent of trees and shrubs is each <10%.
Terrestrial	Natural / Semi-Natural	Non-Forerst	Shrubland	Lands where the majority of woody vegetation cover is <5m in height less and where woody vegetation >=10% canopy cover. Dominant vegetation is evergreen or deciduous.
Terrestrial	Natural / Semi-Natural	Non-Forerst	Snow and Ice	Lands with majority aerial extent comprised of snow and/or ice, majority of the year.
Terrestrial	Natural / Semi-Natural	Non-Forerst	Wetland	Seasonally flooded wetlands dominated herbaceous or shrub vegetation, collectively >=10% canopy cover. Wetland obligates are common.
Terrestrial	Cultural	Forest	Plantation Crop	Lands dominated by trees (>= 10% tree canopy cover) and where cultural crops make up the majority of tree cover. Crops include fast-growing trees such as rubber, oil palm, and others, with crops on relatively short rotations.

Figure 2.11 Primitives and typology used for classification (SERVIR-Mekong, 2016)

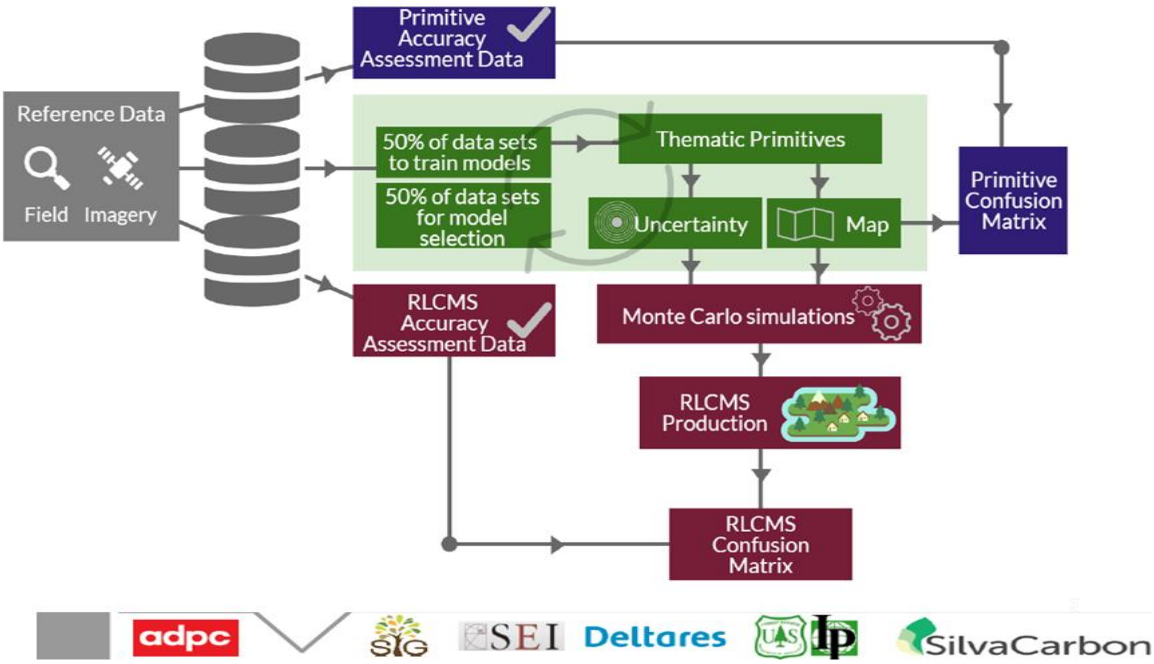

Figure 2.12 Accuracy assessment of land cover classification in the RLCMS (SERVIR-Mekong, 2016)

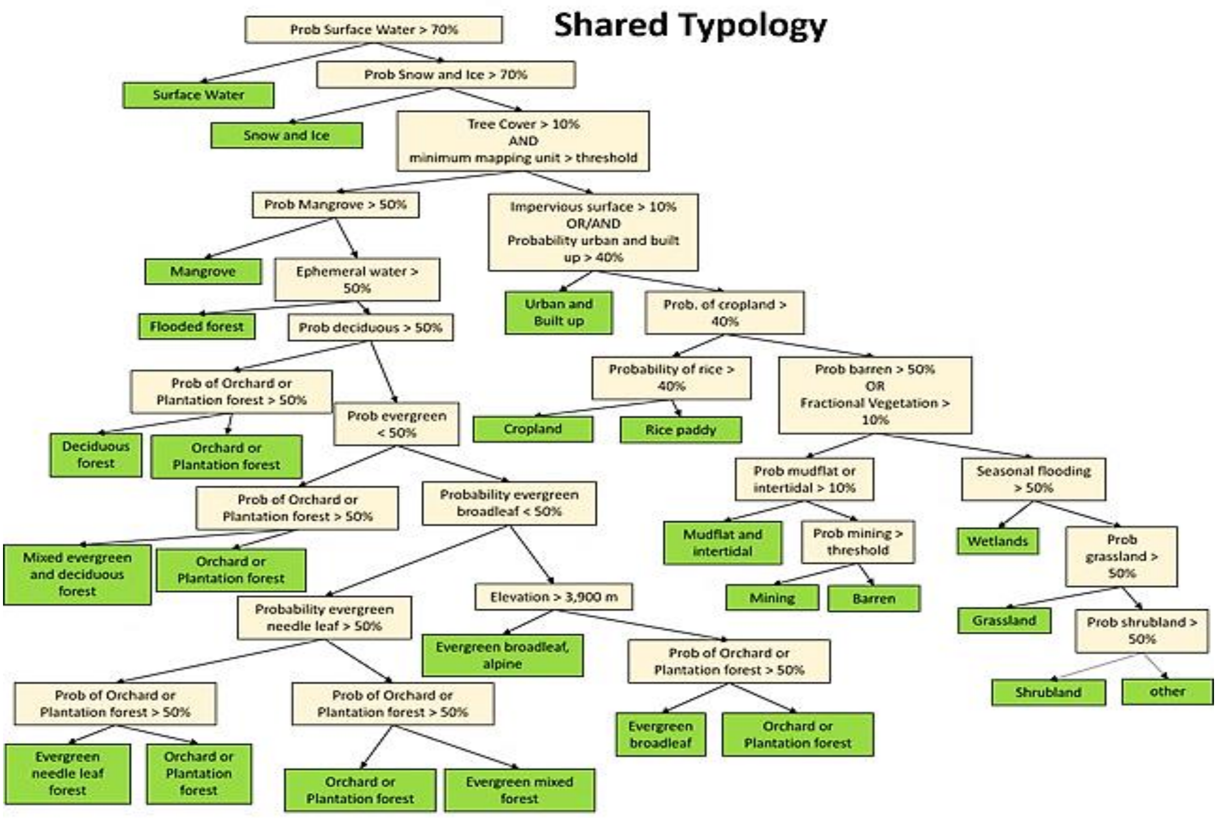

Figure 2.13 Decision tree for assigning land cover classes in the RLCMS (SERVIR-Mekong, 2016)

2.5. Modelling rainfall-runoff and erosion scenarios

2.5.1. Hydrological and erosion modelling

The Limburg Soil and Erosion model (LISEM) has been shown to give detailed interpretations of hydrological processes in small and medium-sized catchments. It is very reliable in simulating runoff, sedimentation, and transportation of sediments from single rainfall events (Rahmati et al., 2013). There is a possibility of calibrating infiltration, base flow and initial soil conditions in the model which are necessary to have a good representation of the in-situ catchment conditions. Model calibration makes results useful when setting up a model to obtain realistic results. LISEM is also able to identify the controlling physical properties and human impacts which have the most impact on the runoff and erosion (de Barros et al., 2014).

LISEM, a physically-based hydrological and erosion model, was used to carry out runoff and soil loss simulation in this research. It can be used for scenario modelling and spatial planning purposes (De Roo et al., 1996; Jetten, 2016). It was designed for catchments with relatively small sizes of a few km^2. The descriptive of rainfall-runoff processes which LISEM simulates include interception, infiltration, surface water storage and surface flow of water in one dimension or two dimensions, detachment of soil particles, and sediment transport and deposition. The choice of using this model was driven by its ability for the model to carry out this processes to fit the characteristics of the catchment. The model can be calibrated with the use of the physical properties measured in the study area. It was also chosen because it can simulate different user-defined land use and rainfall scenarios. Scenario modelling can easily be achieved by adjusting the input data in the case that data is difficult to obtain due to complex topography of the watershed. Another ability of LISEM is the ease of incorporating different land use and conservation management scenarios in rainfall-runoff processes in a catchment (De Roo et al., 1996). The processes of rainfall-runoff modelling in LISEM is shown in Figure 2.14. Green and Ampt infiltration equation and Manning's equation were used for flow routing. While carrying out the simulations, flow from each cell was routed using the diffusive wave method which uses the DEM as the flow network.

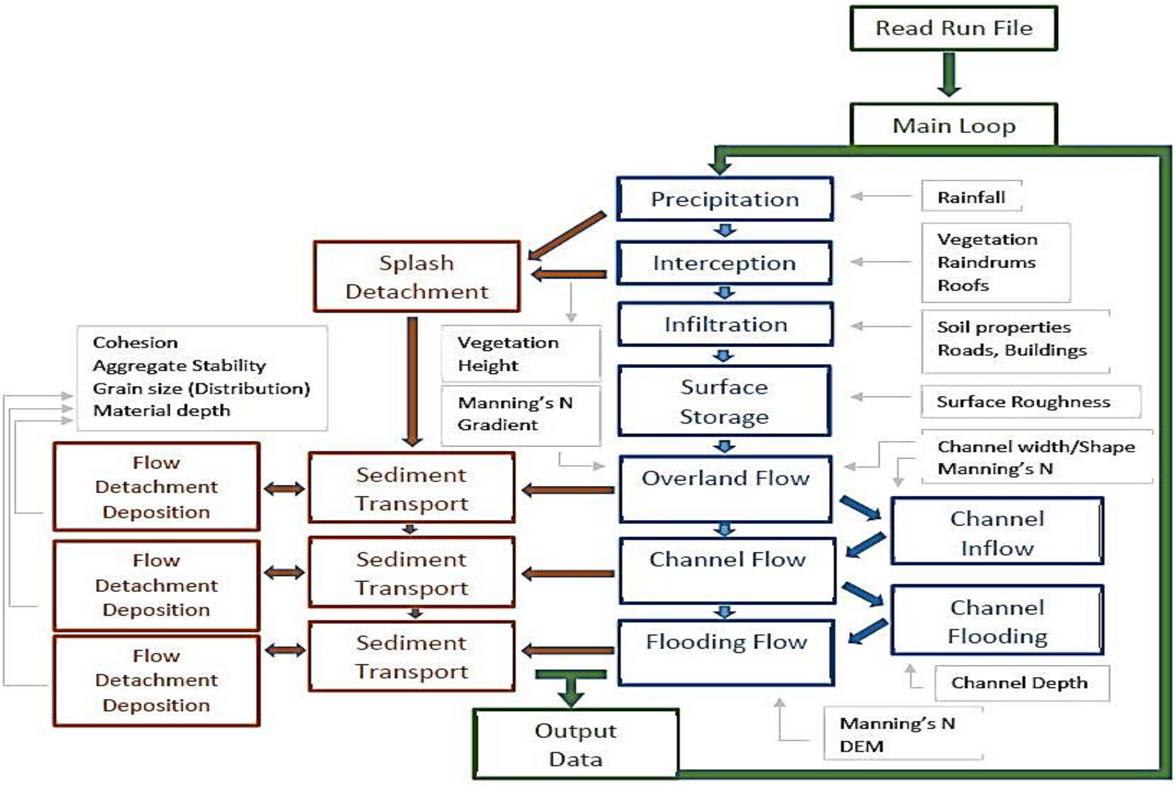

Figure 2.14 LISEM model simulation (Jetten, 2016)

2.5.2. Land management scenarios implemented in the watershed

In the study area, some conservation measures are being implemented. Agricultural practices are prohibited on higher slopes, and all roads leading to those areas have been blocked. As part of watershed restoration efforts, reforestation by teak tree planting has been introduced by the land development authorities. As part of a local project known as the Royal project initiated by the immediate past king after a disastrous flooding event in August 2001, land management strategies are in place in many parts of Thailand. They have decided to minimise agricultural practices in the study area as part of measures to control excessive flooding and erosion in the area. Some of this practices being implemented in the study area are:

1. Farmland abandonment: Most of the areas in the watershed are being abandoned to let the land regrow into natural forests.
2. Reforestation: Teak plantations are increasing in the area to improve canopy cover. This type of tree grows very tall and has broad leaves. The erosive power of rainfall is assumed to be significantly reduced in areas where this tree is being planted.
3. Terracing: In places where farming must be done on slopes, terracing on the slopes helps to reduce the slope gradient, so that excessive runoff does not lead to eroded hills.
4. Mulching: Retaining harvest plant residues for covering the topsoil.

Figure 2.15 Teak plantations

Figure 2.16 Terracing

Figure 2.17 Mulching with maize residue

Multiplication factors were used to adjust the properties to incorporate the conservation scenarios in the model. These multiplication factors were obtained from Hessel et al., (2008), a study in which LISEM was used for soil conservation studies in an agricultural catchment in Kenya. There are similarities to this study as it was done in a tropical climate similar to Thailand. The multiplication factors used for the LISEM input are presented in Table 2.2.

Table 2.2 Effect of land management implemented in LISEM

Conservation measures	Input properties	Multiplication factors/adjustments
Terracing and mulching	Slope gradient	Reducing slopes higher than 30% to 15% on cropland areas
	Random roughness	1.4
	Vegetation cover	1.2
	Leaf area index	1.1
	cohesion	1.1
	Saturated hydraulic conductivity	2.6
Reforestation	Land cover type	Converting cropland and bare areas to forests on slopes higher than 30%.
	All physical properties	1

3. RESULTS ON VEGETATION COVER AND LAND COVER CHANGE ANALYSIS

3.1. Land cover change analysis

Figures 3.1, 3.2 and 3.3 show the land cover classification of 2000, 2010 and 2016 respectively as obtained from the SERVIR- Mekong Regional Land Cover Monitoring System (RLCMS) by the procedures outlined in section 2.4. The land cover maps were generated from Landsat 30-m spatial resolution satellite imagery.

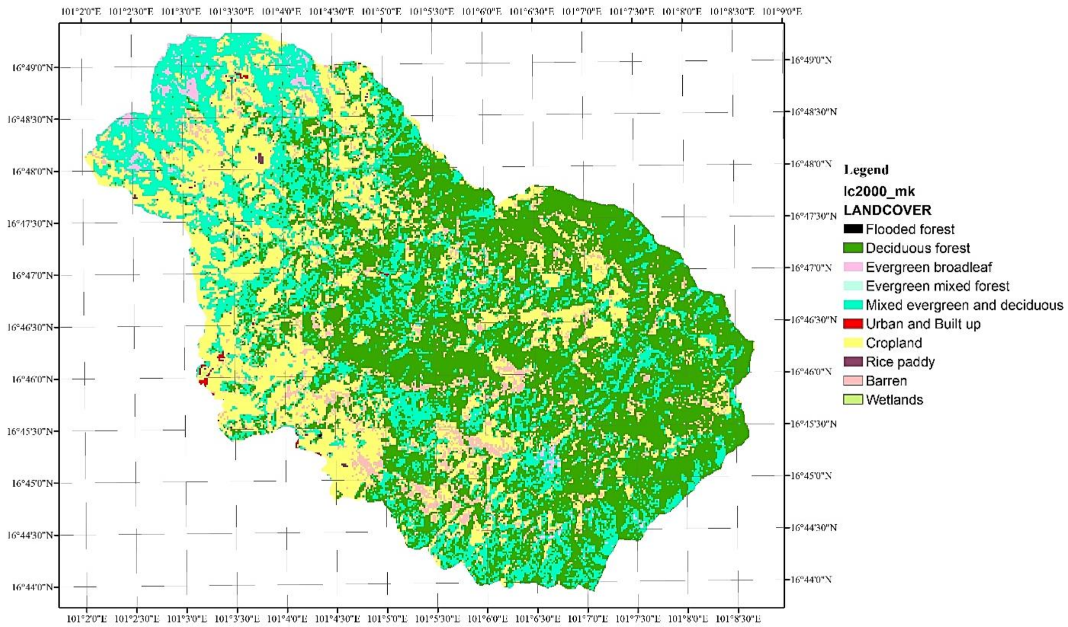

Figure 3.1 Land cover as at 2000 (SERVIR-Mekong database)

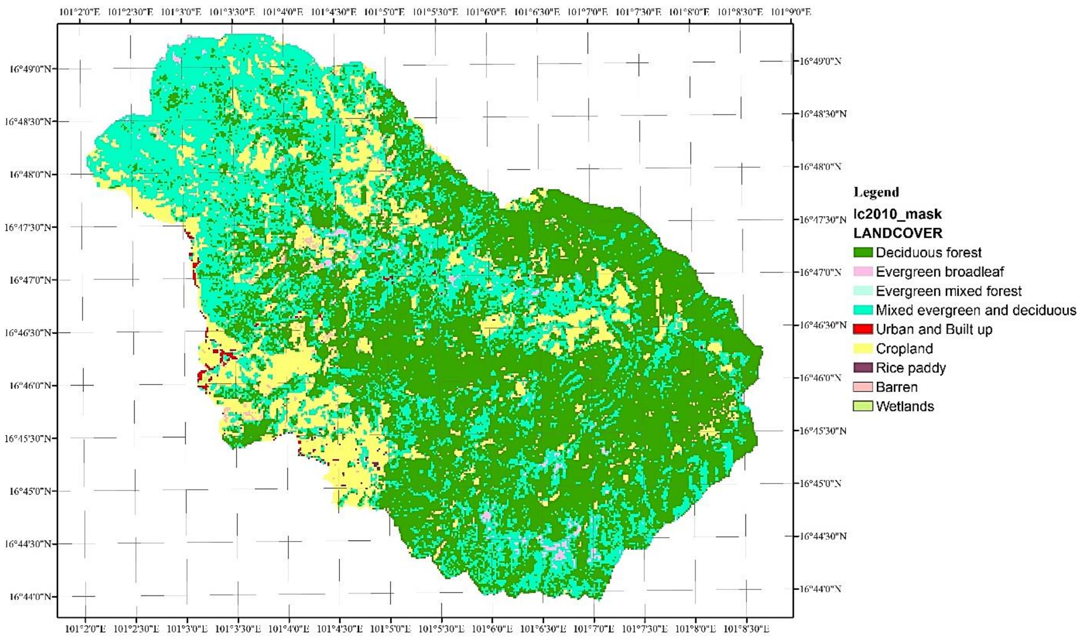

Figure 3.2 Land cover as at 2010 (SERVIR-Mekong database)

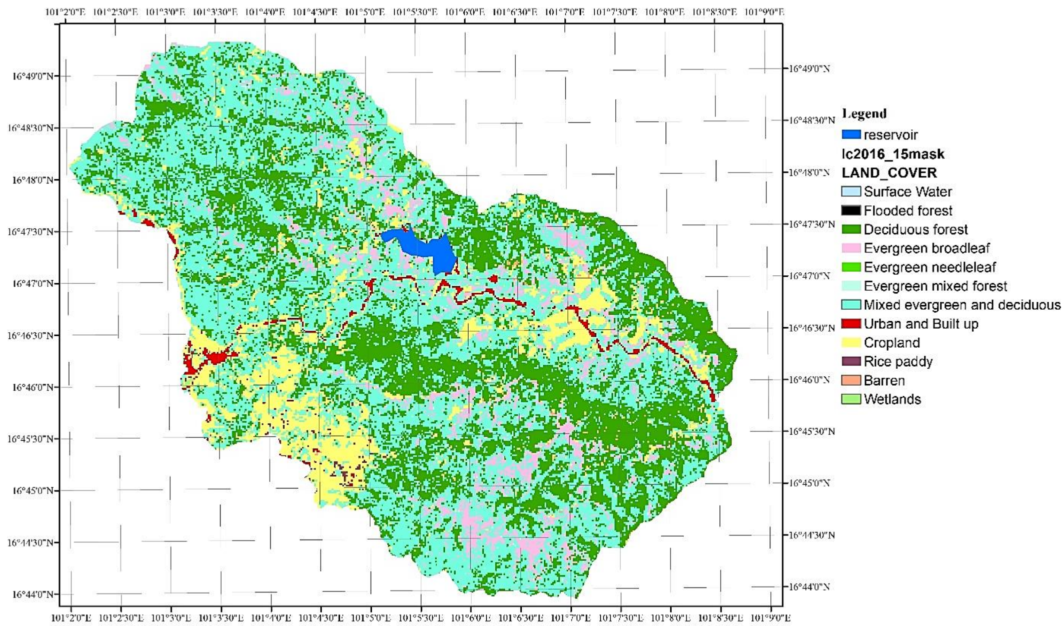

Figure 3.3 Land cover as at 2016 (SERVIR-Mekong database)

Table 3.1 Change in area from 2000 to 2016 in square kilometres and percentage of the total area

Land cover class	Area (km^2) in 2000	Area (km^2) in 2010	Area (km^2) in 2016	Percentage of total area (%) in 2000	Percentage of total area (%) in 2010	Percentage of total area (%) in 2016
Deciduous forest	30.44098	36.00653	22.99752	**42.111**	**49.699**	**31.756**
Mixed evergreen and deciduous	18.72010	24.31083	34.72937	**25.897**	**33.555**	**47.956**
Evergreen mixed forest	0.02374	0.03115	0.37469	**0.033**	**0.043**	**0.517**
Evergreen broadleaf	0.79231	0.57526	5.21498	**1.096**	**0.794**	**7.201**
Cropland	18.54611	10.64141	7.64256	**25.656**	**14.688**	**10.553**
Barren	3.60283	0.63698	0.18637	**4.984**	**0.879**	**0.257**
Rice paddy	0.06106	0.04475	0.12384	0.085	0.062	0.171
Flooded forest	0.00410	0	0.04490	0.006	0	0.062
Surface Water	0	0	0.23052	0	0	0.318
Wetlands	0.00630	0.01262	0.03316	0.009	0.017	0.046
Evergreen needle leaf	0	0	0.00095	0	0	0.001
Urban and Built-up	0.08963	0.19025	0.84125	0.124	0.263	1.162

Table 3.1 shows the change in area from 2000 to 2016. Figure 3.4 shows a reclassification of all the land cover types to 3 broad classes (forest, agriculture and barren). Forested areas have increased while agricultural areas have reduced. Barren areas have been reduced from 3.6 square kilometres in the year 2000 to 0.18 square kilometre in the year 2016. Agricultural fields have reduced from 18.55 square kilometres in 2000 to 7.64 square kilometres in 2016. Forest areas have expanded from 45.34 square kilometres in the year 2000 to 57.67 square kilometre in the year 2016. There is a significant increase in forest areas from 2000 to 2016. By adding up the percentage area of forest types represented in Table 3.1, as at 2016, about 80% of the watershed is covered by forests compared to 69% in 2000.

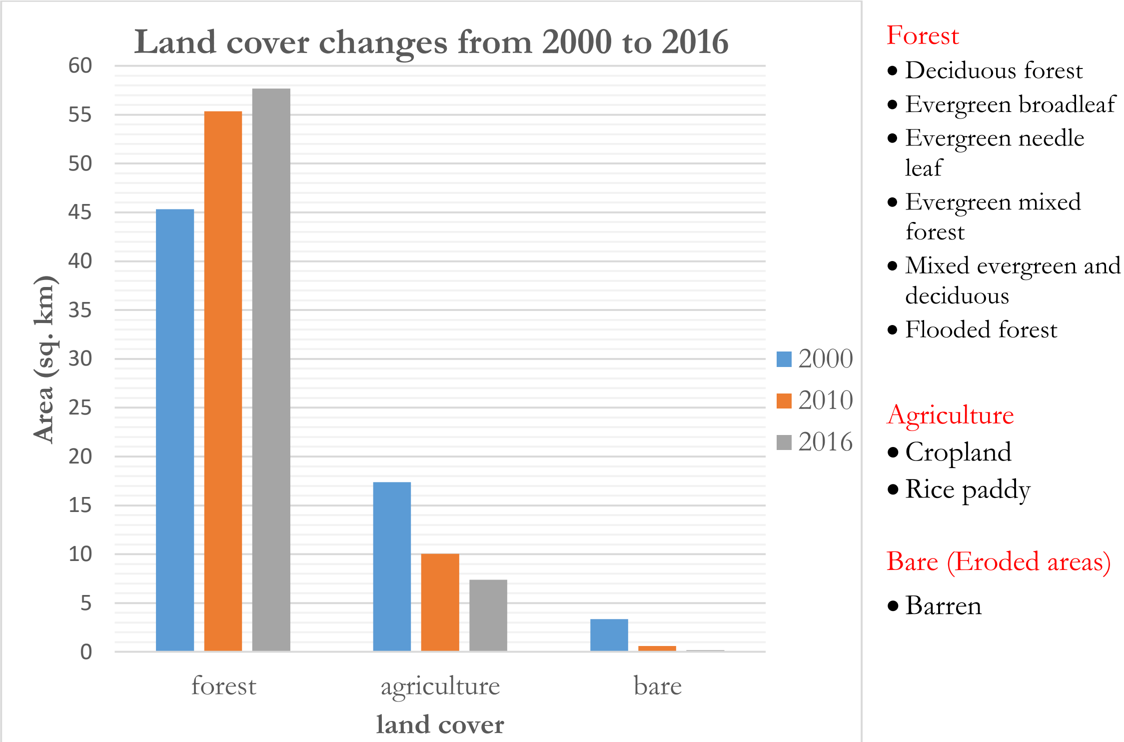

Figure 3.4 Areal changes in land cover from 2000 to 2016

3.2. Canopy/vegetation cover estimation

From the method of estimating vegetation cover explained in section 2.3.2, vegetation cover was predicted for the entire watershed using remote sensing parameters. To compare the values of NDVI from remote sensing and the NDVI measured on the field, a linear regression was done for field NDVI and vegetation cover percentage from the field. The relationship is represented in Figure 3.5. Vegetation cover used as input for the prediction was adjusted based on the relationship between field NDVI and field measured vegetation cover.

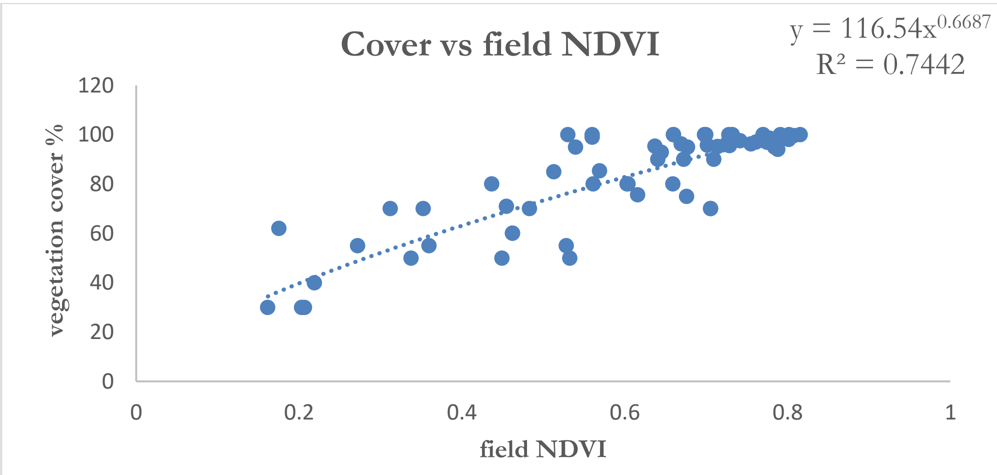

Figure 3.5 Relationship between field-measured NDVI and vegetation cover

The maps of Figure 3.6 show vegetation cover distribution for the area as obtained by this method. The predicted vegetation cover in the area is seen to be between 26 to 99 percent. The relationship between the vegetation cover and vegetation indices served as training values for classifying images while implementing random forest regression. The training values were used to create time series predictions of vegetation from satellite images of 2000 and 2017. The vegetation cover prediction process used the composite image. The training accuracy achieved for the prediction was 95.24%. The predicted vegetation cover percentage for the dates in 2000 and 2017 are shown in Figure 3.6.

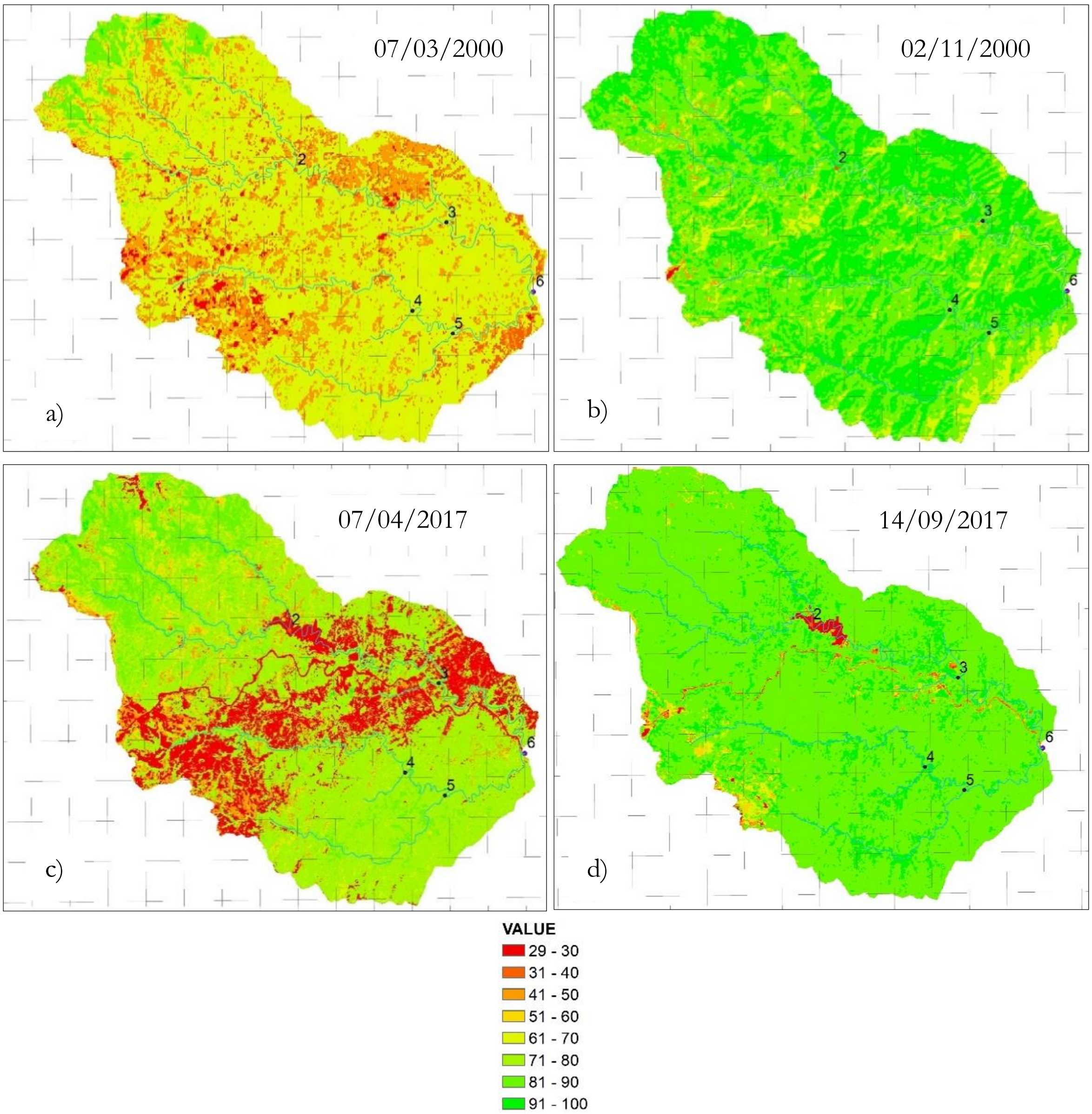

Figure 3.6 Derived vegetation cover maps from the dry and wet season for 2000 (a & b) and 2017 (c & d)

4. RESULTS ON THE EFFECTS OF RAINFALL INTENSITY AND LAND COVER CHANGES ON RUNOFF AND SOIL LOSS

Scenarios were created for running the LISEM model to assess the runoff, sediment and soil loss patterns in the watershed. The scenarios were based on rainfall intensity, seasonal vegetation cover and long-term land cover changes. The vegetation cover change scenarios (low vegetation and high vegetation cover) were based on results from the vegetation cover prediction using random forest regression on satellite images from 2000 and 2017 as shown below. The dates are chosen to represent the beginning and the end of the planting season/beginning and end of the rainfall season in the area. The land cover classification corresponding to the image period was selected that is, 2000 and 2017.

Table 4.1 Scenario selection

Vegetation cover changes	**Land cover changes**	
	2000	**2017**
Low vegetation cover and beginning of rainfall season **(LV)**	07/03/00 (March) **(2000 LV)**	07/04/17 (April) **(2017 LV)**
High vegetation cover and end of rainfall season **(HV)**	02/11/00 (November) **(2000 HV)**	14/09/17 (September) **(2017 HV)**

4.1. Data preparation to run hydrological model (LISEM)

The base maps required to run the LISEM model for simulating runoff and sediment processes are land use/cover, soil, vegetation cover and elevation maps. From these base data, the attribute maps of the watershed for which any GIS program can be used. PCRaster was used to create the input maps with the use of a script. Maps were created at a spatial resolution of 15 metres. The rainfall-runoff model (LISEM) was run with event rainfall data and with a time step of 10 minutes for 16 hours 30 minutes' duration.

4.1.1. Rainfall

Daily rainfall data from 1953 -2017 was collected from the meteorological station in Lomsak, which was the closest to the study area. Satellite-derived Hourly rainfall from 2000 to 2017 was also obtained for the study area from PERSIANN global hourly rainfall database developed by Centre for Hydrometeorology and Remote Sensing (CHRS) unit, University of California – Irvine (obtained from http://chrsdata.eng.uci.edu). Daily and hourly rainfall data were then used for a Gumbel return period analysis, results which are shown in Figure 4.1. An Intensity-duration-frequency (IDF) curve was obtained from rainfall distribution studies done by Rittima et al. (2013) for the various provinces in Thailand. Rainfall intensity values were then extracted and used to derive 15-minute interval intensities for 5, 10, 25, 50 and 100-year return periods. Values obtained from the IDF rainfall curves were compared with the results from the Gumbel analysis results to arrive at the appropriate duration. A 4-hour duration rainfall was chosen as that duration gave the similar amount of rainfall as compared with results from the Gumbel distribution. Table 4.2 shows the maximum rainfall amount for the return periods considered which served as the limiting values for the rainfall design storms using the IDF curves.

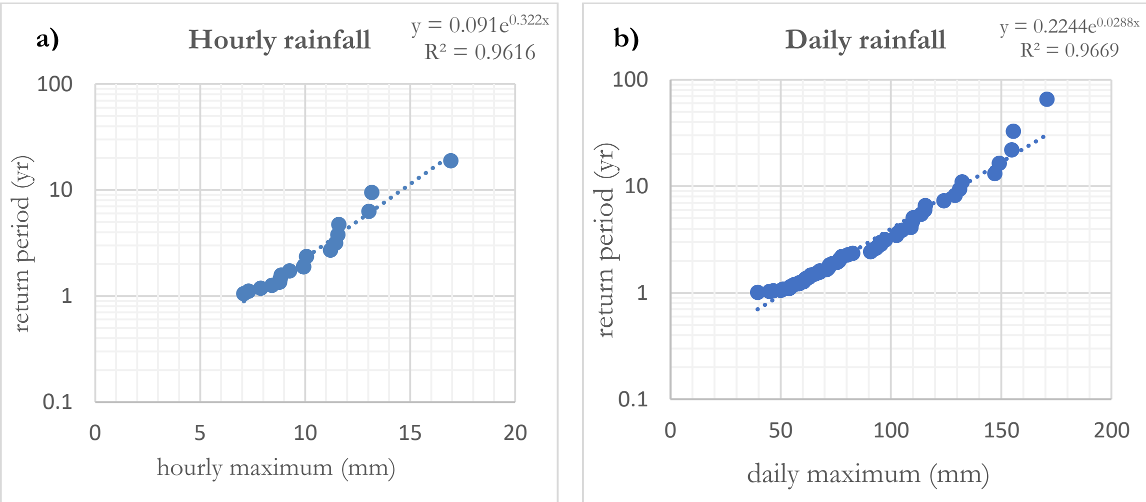

Figure 4.1 Return period of a)hourly and b)daily rainfall data for the study area

Table 4.2 Maximum rainfall for design return periods

Return period	R. Prob	L. Prob	y	1 hr (mm)	24 hr (mm)
2	0.5	0.5	0.37	**9.96**	**80.76**
5	0.2	0.8	1.50	**12.58**	**110.51**
10	0.1	0.9	2.25	**14.31**	**130.21**
25	0.04	0.96	3.20	**16.50**	**155.10**
50	0.02	0.98	3.90	**18.12**	**173.56**
100	0.01	0.99	4.60	**19.74**	**191.88**

Right probability =1/ Return period (T).

Left probability = 1- Right probability

y = -ln (-ln (left prob.))

4.1.1.1. Rainfall scenarios

The LISEM model requires high temporal resolution event-based rainfall as input for the runoff modelling. Rainfall data in the required resolution was unavailable as the minimum rainfall data available was hourly-based. The rainfall data was derived from the Intensity-duration-frequency (IDF) curves from the studies done by Rittima et al. (2013), who carried out on rainfall studies in Thailand, to generate rainfall data in which less than one-hour resolution. The IDF curves for Phetchabun province, in which the watershed is located, is presented in Figure 4.2. The values obtained from the IDF curve were readjusted to fit a realistic rainstorm in which there are gradual increases and decreases in rainfall intensity. Creation of the design rainfall storms was done by using the alternating block method according to (Yen & Chow, 1980). The values of rainfall intensities are obtained from the curves and then alternated with the maximum intensity peaking at the middle of the total duration. Fifteen-minute resolution rainfall events were created for 5, 10, 25, 50 and 100-year return periods. Table 4.3 shows the rainfall intensities for a four-hour duration rainfall for the selected return periods. Figure 4.3 shows the selected rainfall scenarios used as input for the rainfall-runoff modelling with LISEM.

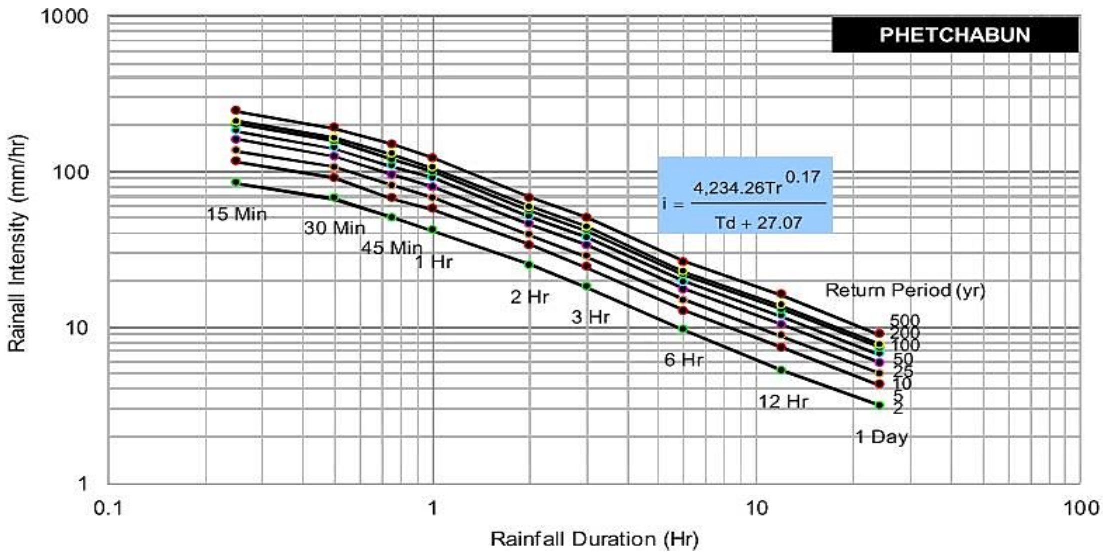

Figure 4.2 Rainfall Intensity-Duration-Frequency curve of Phetchabun District, Thailand (Rittima et al., 2013)

Table 4.3 Design rainfall storms obtained from the IDF curves using alternate block method

Time (min)	15	30	45	60	75	90	105	120	135	150	165	180	195	210	225	240
5yr	0.099	0.1	2	4	10	30	70	110	30	20	10	4	1.5	0.341	0.01	0
10yr	0.578	0.79	2	6	17	42	65	145	42	15	10	5	1.05	0.64	0.492	0.33
25yr	0.57	0.7	6	7	13	50	90	160	50	15	9	5	2.3	0.69	0.24	0.02
50yr	1.40	2.36	3.4	6	11	60	110	190	60	23	8	4.6	3	1.64	1.1	0.9
100yr	0.122	1.08	4.8	6.9	13	80	130	210	80	25	9.5	5.8	3	0.67	0.978	0.35

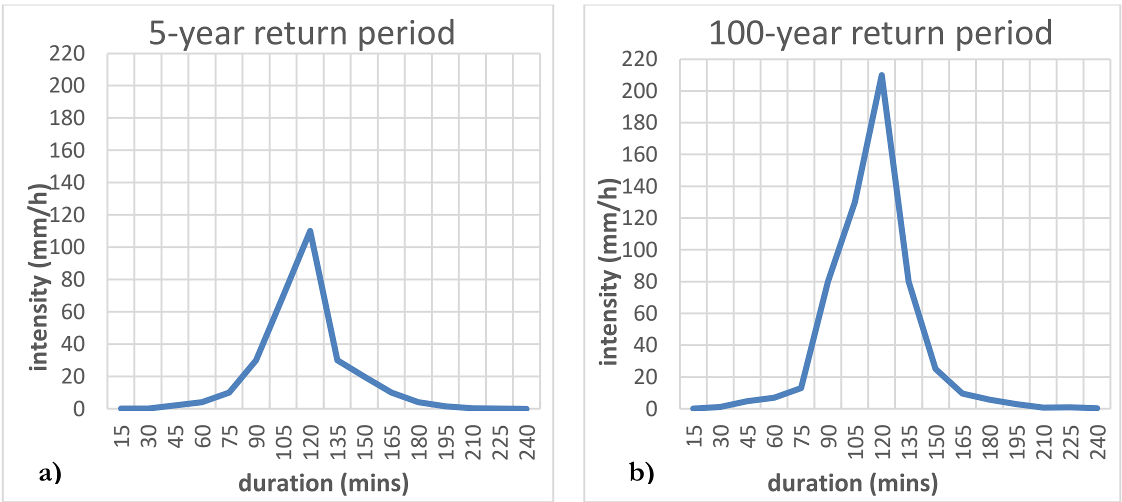

Figure 4.3 a)5-year and b) 100-year return period rainfall storms

4.1.2. Topography

The elevation data of the study area was derived from digitised contour lines with 5-metre spatial resolution and 1-metre vertical interval provided by the Land Development Department, Phetchabun, Thailand. Significant derivatives from the DEM required for the model include slope gradient, local drainage direction and stream network. The DEM for the study area is shown in Figure 4.4.

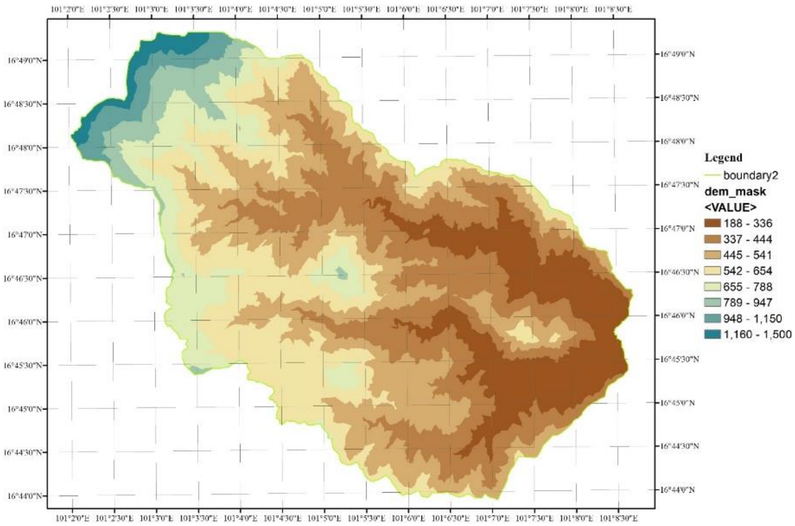

Figure 4.4 Digital elevation model

4.1.3. Soil

Sixteen soil samples were collected from the study area for laboratory analysis at Naresuan University in Thailand. The results of the laboratory tests carried out on the soil obtained from the various land use types in the study area with the procedures outlined in chapter 2 (section 2.2) is presented in Figure 4.5 below. Six soil samples were taken in agriculture fields, two from bare fields, six from forest areas and two from grassland fields. Saturated hydraulic conductivity (ksat), bulk density (BD) and porosity tests were carried out with the using the soil samples. The saturated hydraulic conductivity of soil collected from the forest land use types were significantly higher than form other land use types. Saturated hydraulic conductivity values as high as 125 mm/hr were obtained for soils collected from forest land cover types. The agricultural land cover had less than 10mm/hr while bare areas had saturated hydraulic conductivity of 2mm/hr and below. Porosity was also higher in forests than in other land cover type. For forest areas, porosity was as high as 53%. Agricultural areas were shown to have a porosity of about 29% to 43 % which may be due to tillage of the soil during planting. Bulk density was relatively constant for all land cover types ranging from 1.4 g/cm^3 to 1.8 g/cm^3. The mean values are shown in the box plot by the symbol '**X**' while the sample values are shown by '**o**'.

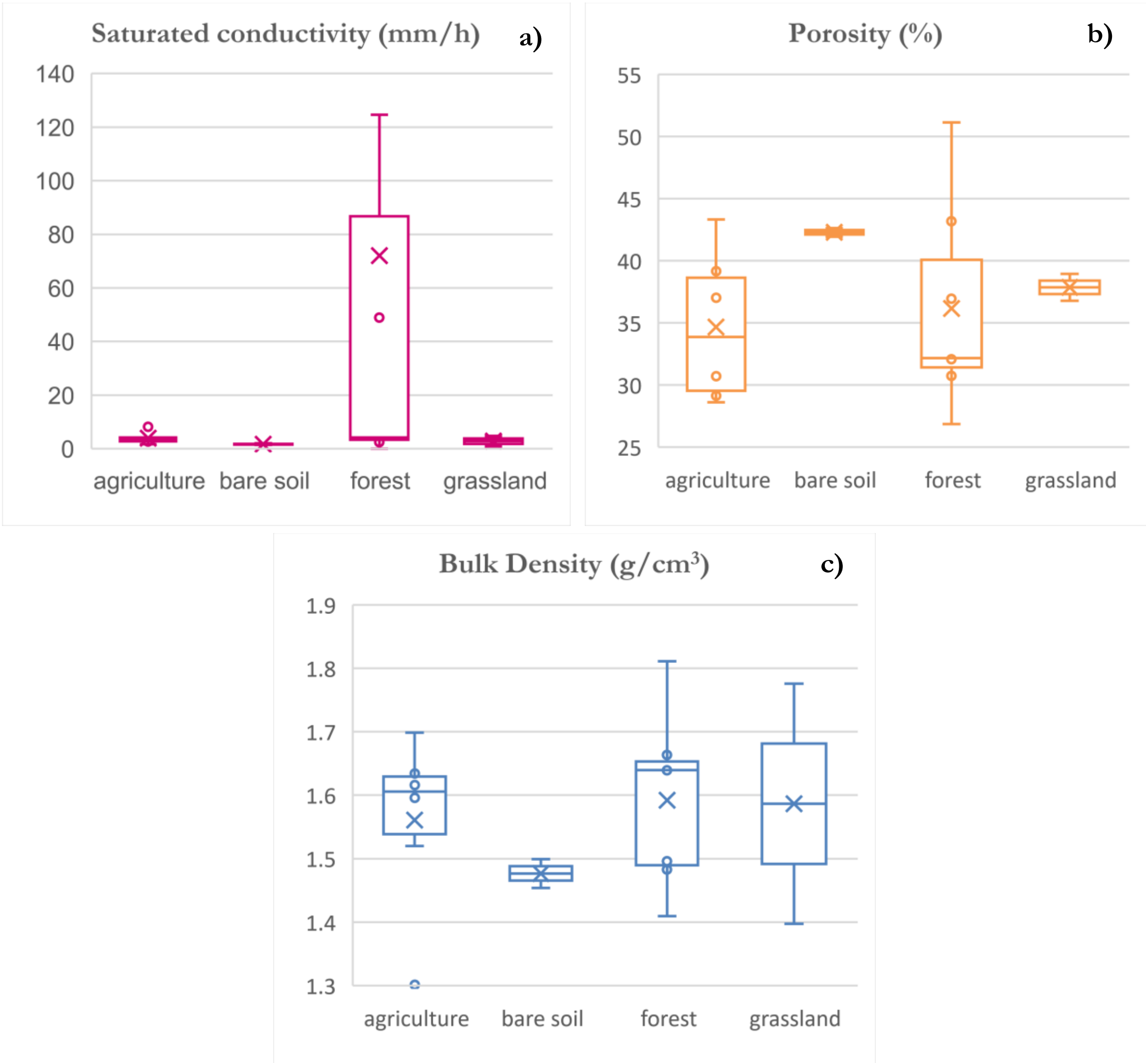

Figure 4.5 a), b), c) Soil physical properties of different land use types

The soil properties for LISEM were obtained from the soil laboratory results. Other soil units not tested were derived from the LISEM manual for different soil textures (Jetten, 2016), and the Saxton and Rawls pedo-transfer function (Saxton & Rawls, 2006) and from a previous study done in the area (Shrestha & Jetten, 2018; Suriyaprasit & Shrestha, 2007). The properties required for each soil unit include soil cohesion, soil moisture, field capacity, soil suction and soil particle size. The soil texture types in the study area were clay loam (CL), silty loam (SL), clay (C), silty clay loam (SiCL) and silty clay (SiC). These were classified into different units based on the geomorphological properties from studies done by Solomon (2005). From the soil unit map in Figure 4.6, Table 4.4 was derived, and soil property maps were created. These input data were then used to run different scenarios of vegetation, land cover and rainfall changes from 2000 and 2017.

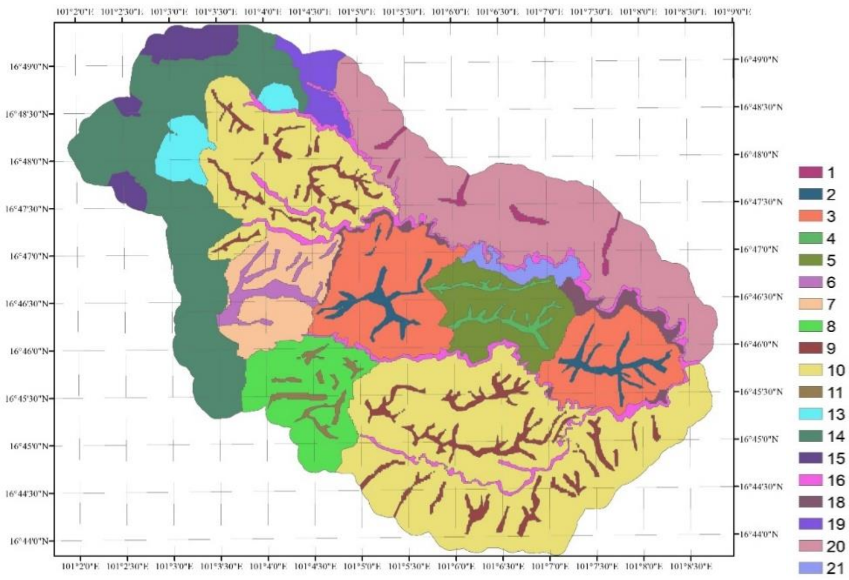

Figure 4.6 Soil unit map (Solomon, 2005)

Table 4.4 Soil properties for each soil unit

Unit	Soil texture	Cohesion (KPa)	Saturated hydraulic conductivity (mm/h)	Porosity (cm^3/cm^3)	Soil suction (cm)	Field capacity (cm^3/cm^3)
1	CL	3.00	4.2	0.472	50	0.35
2	CL	3.00	4.2	0.472	50	0.35
3	CL	10.00	4.2	0.472	50	0.35
4	SL	2.00	17.4	0.45	40	0.179
5	C	10.00	2.5	0.488	50	0.42
6	SiCL	10.00	25	0.51	40	0.379
7	CL	10.00	4.2	0.472	50	0.35
8	CL	10.00	4.2	0.472	50	0.35
9	C	3.00	2.5	0.488	50	0.42
10	CL	10.00	4.2	0.472	50	0.35
11	SiC	10.00	13	0.532	40	0.416
13	SiC	10.00	13	0.532	40	0.416
14	SiC	10.00	13	0.532	40	0.416
15	C	3.00	2.5	0.488	50	0.42
16	channels	3.00	49.6	0.45	10	0.18
18	CL	10.00	4.2	0.472	50	0.35
19	SiC	10.00	13	0.532	40	0.416
20	CL	10.00	4.2	0.472	50	0.35
21	CL	10.00	4.2	0.472	50	0.35

4.1.4. Land cover

The annual land cover and vegetation cover maps as presented in section 3.1 and 3.2 were used to derive land cover properties required for the model. These are plant height, surface roughness, Manning's n, root strength, leaf area index. Based on the land cover classification, the properties in Table 4.5 were derived from the Lisem manual (Jetten, 2016). The addition root strength of the soil was obtained as a function of the vegetation cover. Leaf area index was derived using the vegetation cover maps using Equation 2.4 below. The maximum value of vegetation cover is taken as 0.99 to avoid negative values.

$$LAI = ln(1 - Cover)/-0.4 \quad \text{......} 2.4$$

Openstreet® maps database (https://www.openstreetmap.org/export#map=13/16.7630/101.1932) was the source of the road network map for the area. The vector road map was converted to raster format and subsequently converted to PCRaster format.

Table 4.5 Land cover properties for each land cover unit

Land cover unit	Plant height (m)	Random roughness (mm)	Manning's n
Surface Water	0	0.1	0.05
Flooded forest	19.5	1	0.4
Deciduous forest	19.5	1	0.4
Evergreen broadleaf	19.5	1	0.4
Evergreen needle leaf	19.5	1	0.4
Evergreen mixed forest	19.5	1	0.4
Mixed evergreen and deciduous	19.5	1	0.4
Urban and Built up	0	0.5	0.05
Cropland	1	1	0.03
Rice paddy	1	1	0.03
Barren	0.05	0.5	0.01
Wetlands	0.5	1	0.1

4.2. Hydrological analysis

A PCRaster script (presented in Appendix 2) was used to create the input data for LISEM. The slope gradient map (Figure 4.7) was then used to derive the local drainage direction map which defined flow direction pattern of the basin which was then used to derive the stream order of the watershed outlining the drainage pattern (Figure 4.8). The drainage pattern is dendritic suggesting that the lithology of the area is relatively homogenous and the base rocks are resistant to flow (Zende et al., 2018). The dendritic drainage pattern is shown in stream order map in Figure 4.9. Stream orders of 5 and above were considered to be the primary river channels.

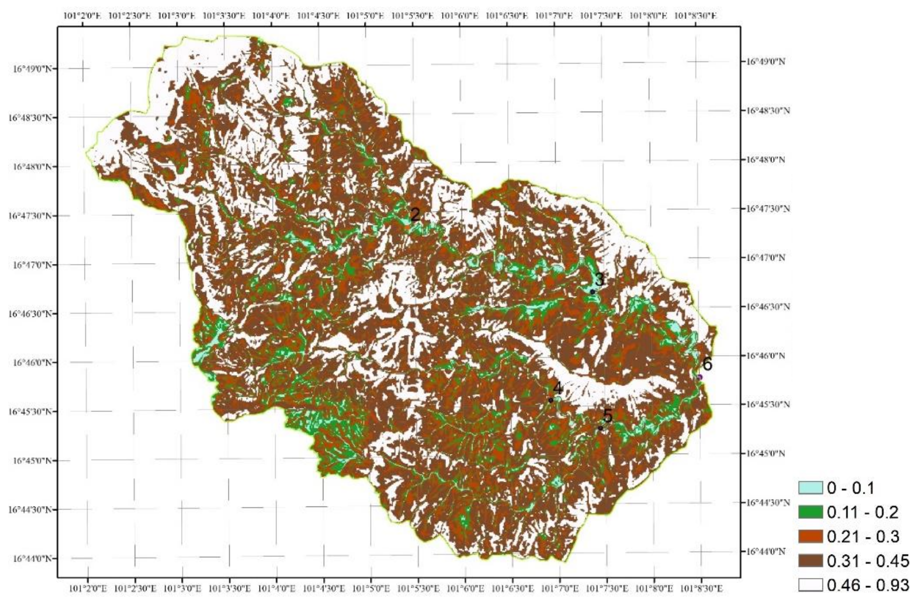

Figure 4.7 Slope gradient

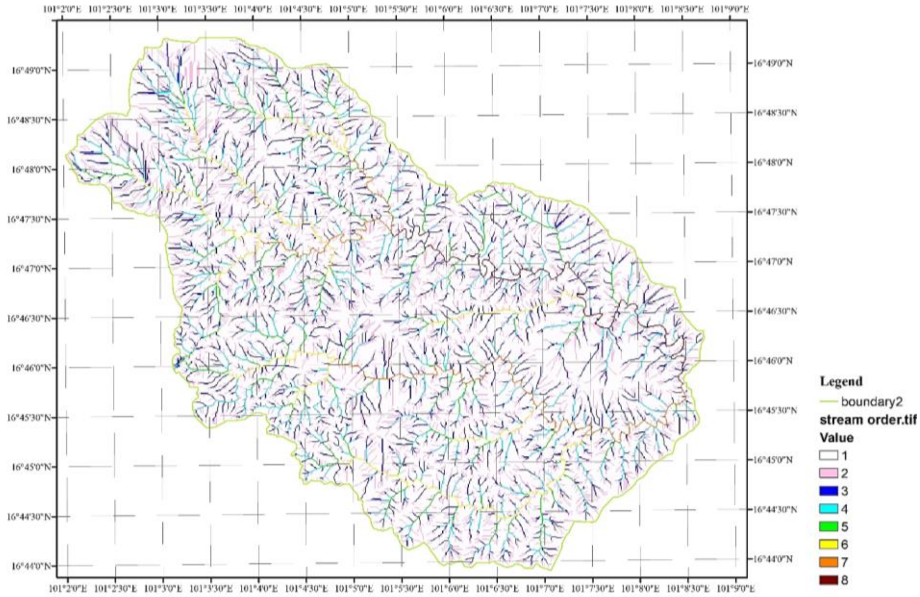

Figure 4.8 Stream order in the watershed

Five catchment outlets were defined as shown in Figure 4.9 to assess the runoff and sediment output from the watershed. They are:

- Point 2: the reservoir inlet and output of majorly forest areas and hillslopes.
- Point 3: output of areas which are mainly agricultural and forest areas but discharge is artificially-controlled by the reservoir outlet discharge.
- Points 4 and 5 is output from majorly agricultural fields. These areas are on lower slopes.
- Point 6 is the primary outlet for the whole watershed.

The catchment area of the outlets is as shown in Table 4.6 below. More attention will be on outlets 2 and 5 for comparing the output from forest and agricultural areas in the watershed.

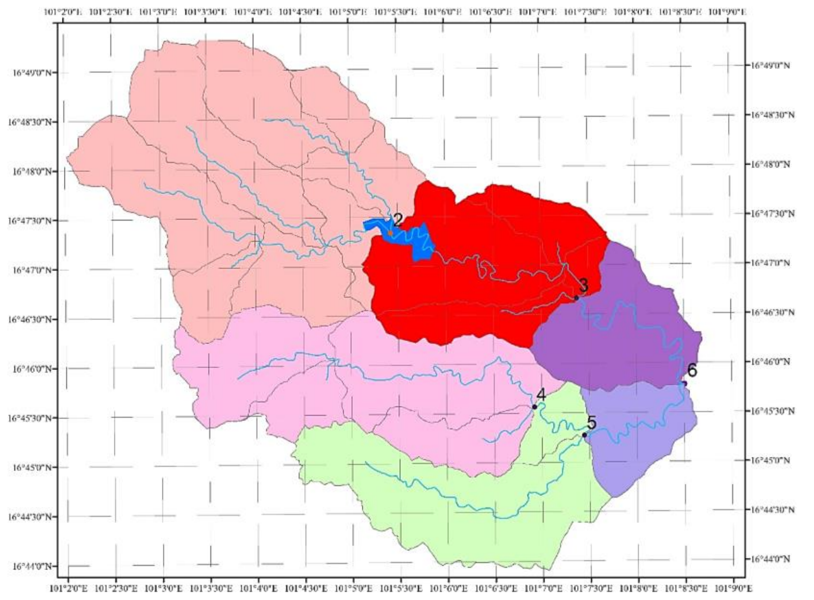

Figure 4.9 Defined catchment outlets along the stream network

Table 4.6 Catchment area of defined catchment outlets

Outlets	**2**	**3**	**4**	**5**	**6**
Catchment Area (ha)	2324.226	3356.846	1399.489	2424.495	7245.900

Table 4.7 shows a summary of all the data required for both surface runoff and soil loss modelling with LISEM model.

Table 4.7 Summary of input data for LISEM

Input maps		**Description**
Initial maps	DEM map	Digital Elevation Model containing elevation values (m)
	Mask map	Map of the Boundary of the area (value 1)
	LU map	Map containing land cover classification
	Soil map	Map containing soil classification
	Road map	Map of area covered by paved roads (0 and 1)
	per map	Map containing vegetation cover percentage (0 to 1)
	Soil table	Table containing soil physical properties (Ksat, thetaI, psi, coh)
	LU table	Table containing land cover units properties (n, rr, ch)
	Outlet all map	User-defined Sub-catchment outlets defined by the user
Derived maps with PCRaster	ldd map	Local drainage direction. Runoff drainage direction derived from the DEM
	grad map	Sine of the slope gradient derived from the DEM
	Id map	Rainfall zones map which shows rainfall variability. Equals to mask area if no variable
	Outlet map	The watershed main outlet
	Lai map	Leaf Area Index (m2/m2)
	ch map	Map of Plant height per land unit type (m)
	Ksat map	Saturated hydraulic conductivity per soil unit (mm/h)
	thetaI map	Initial soil moisture per soil unit (dimensionless)
	thetaS map	Porosity per soil unit (dimensionless)
	psi map	Soil Suction per soil unit (cm)
	Soil depth map	Soil depth map (mm)
	rr map	Random roughness per land unit (cm)
	n map	Manning's N per land unit (dimensionless)
	hard surface map	Areas with no infiltration (houses, paved roads)
	coh map	Soil cohesion (KPa)
	cohadd map	Additional plant cohesion to the soil from plant roots (KPa)
	d50 map	Grain-size distribution, Median of texture (μm)
	Aggrstab map	Aggregate stability number (dimensionless)
	chancoh map	Channel cohesion (KPa)
	chanwidth map	Channel width (m)
	chandepth map	Channel depth (m)
	chanside map	Angle of channel sidewalls (0 for rectangular or 1 for 45°)
	chanksat map	Channel Ksat for unpaved channels (mm/h)
	changrad map	Sine of the channel gradient
	chanman map	Channel manning's N (dimensionless)

4.3. Surface runoff modelling

4.3.1. Calibration

A 7-hour duration rainstorm measured in the area on the 6th of September 2005 (shown in Figure 4.10) was used to calibrate the model to arrive at the appropriate calibration factors for the physical properties. This rain event has a 2-year return period when compared with the values obtained from the return period analysis using Gumbel distribution. The 3-hourly discharge from the catchment was also measured and the peak discharge for that day was 32.043 m^3/s. The measured discharge at the outlet of the watershed was compared with that predicted by the model (34.06 m^3/s) while adjusting the calibration factors to arrive at the appropriate calibration factors as presented in Table 4.8.

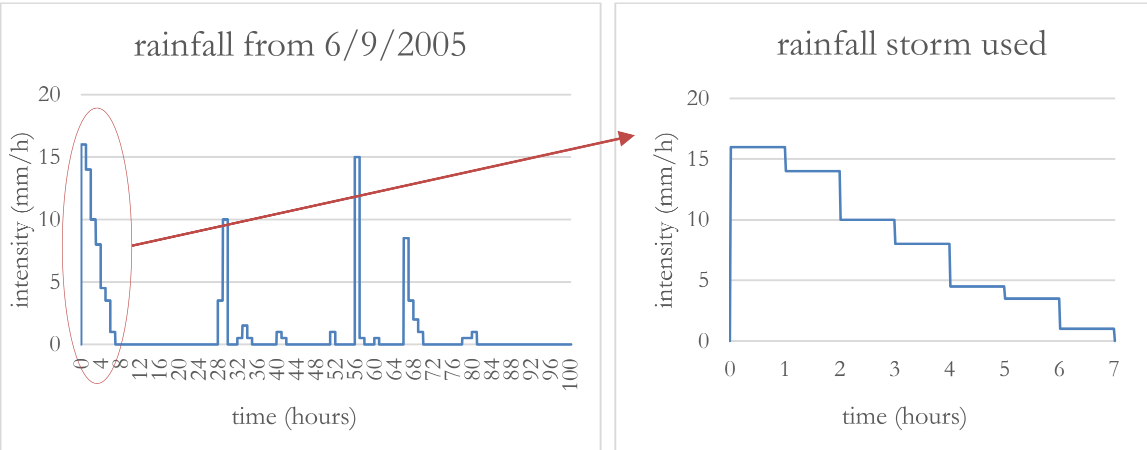

Figure 4.10 Measured rainfall used for calibration

Table 4.8 Calibration factors used in LISEM

Properties	Saturated hydraulic conductivity	Manning's n (slopes)	Manning's n (channels)	Initial soil moisture	Aggregate stability	cohesion
Calibration factors	1.2	1.2	1.0	0.8	1.5	1.2

Table 4.9 shows a summary of the runoff discharge results from the scenarios. The peak discharges, total discharges and the peak discharge to precipitation ratios are shown for the vegetation cover during the dry and wet seasons (LV and HV respectively) for the land cover maps of 2000 and 2017.

Table 4.9 Summary of runoff results from the different scenarios from LISEM

Rainfall intensity return period	**Total rainfall (mm)**	**Land/ vegetation cover scenarios**	**Peak discharge at point 2 (m^3/s)**	**Total discharge (10^3 m^3)**	**Peak discharge/ precipitation ratio (%)**
2yr	57.000	2000 LV	0.009	2.80	0.075
		2017 LV	0.007	3.55	0.094
		2000 HV	0.009	2.32	0.062
		2017 HV	0.007	3.04	0.081
5yr	69.277	2000 LV	15.016	909.68	19.904
		2017 LV	9.585	818.14	17.867
		2000 HV	13.350	804.97	17.613
		2017 HV	8.743	734.58	16.033
100yr	135.433	2000 LV	80.966	4121.34	46.128
		2017 LV	57.334	3888.86	43.441
		2000 HV	76.882	3912.54	43.791
		2017 HV	55.607	3719.76	41.529

The results are obtained from two defined points in the watershed, one from the output from mainly forest areas on high slopes (2) and another from the agricultural fields from lower slopes (5). However, the hydrograph of point 2 which is the input to the reservoir located in the watershed represents the runoff from the mountainous parts of the watershed with higher slope gradients; the hydrograph of point 5 receives runoff discharge from areas with lower slope gradients in which farming is prevalent.

4.3.2. Rain intensity change effect

By running the LISEM model for the land cover of 2017 with high vegetation cover, i.e. in September, with two scenarios of rainfall (5-year and 100-year return period rainfall storms) the differences in runoff discharge results are presented in Table 4.10.

Table 4.10 Surface runoff change for rainfall storms of 2, 5 and 100-year return periods with high vegetation cover in 2017

2017 land cover in the wet season with high vegetation cover scenario	**2yr**		**5yr**		**100yr**	
	Reservoir inlet (outlet 2)	**Agricultural areas (outlet 5)**	**Reservoir inlet (outlet 2)**	**Agricultural areas (outlet 5)**	**Reservoir inlet (outlet 2)**	**Agricultural areas (outlet 5)**
Peak time (hr)	6	6	6.83	7.33	7.67	6.17
Peak discharge (m^3/s)	0.007	0.003	8.743	4.435	55.607	20.338
Total rainfall (mm)	57		69.28		135.43	
Total interception (mm)	3.44		3.43		3.43	
Total infiltration (mm)	53.42		50.74		60.02	
Total discharge (m^3)	$0.003X10^6$		0.735×10^6		$3.72 X10^6$	
Peak discharge/ precipitation ratio (%)	0.081		16.033		41.529	

The duration of the model run was for 16 hours 30 minutes. The 2-year rainstorm hydrograph, as shown in Figure 4.2, shows a peak runoff discharge which is less than **0.01 m^3/s** from both point 2 and 5. A rainstorm of that magnitude does not seem to pose any problems. However, the peak runoff of a 5-year rainfall storm (as seen in Figure 4.2 (b)) from hydrograph 2 is **8.743 m^3/s** at about **6 hours 50 minutes** while that from hydrograph 5 is **4.435 m^3/s** at **7 hours 20 minutes.** In comparison, the peak discharge from a 100-year rainfall storm at point 2 is **55.607 m^3/s** at **7 hours 40 minutes** while that from point 5 is **20.338 m^3/s** at **6 hours 10 minutes**. The hydrograph is shown in Figure 4.2 (c). The catchment area covered by point 2 is almost the same as point 5 (**2324.23 ha** and **2424.50 ha** respectively).

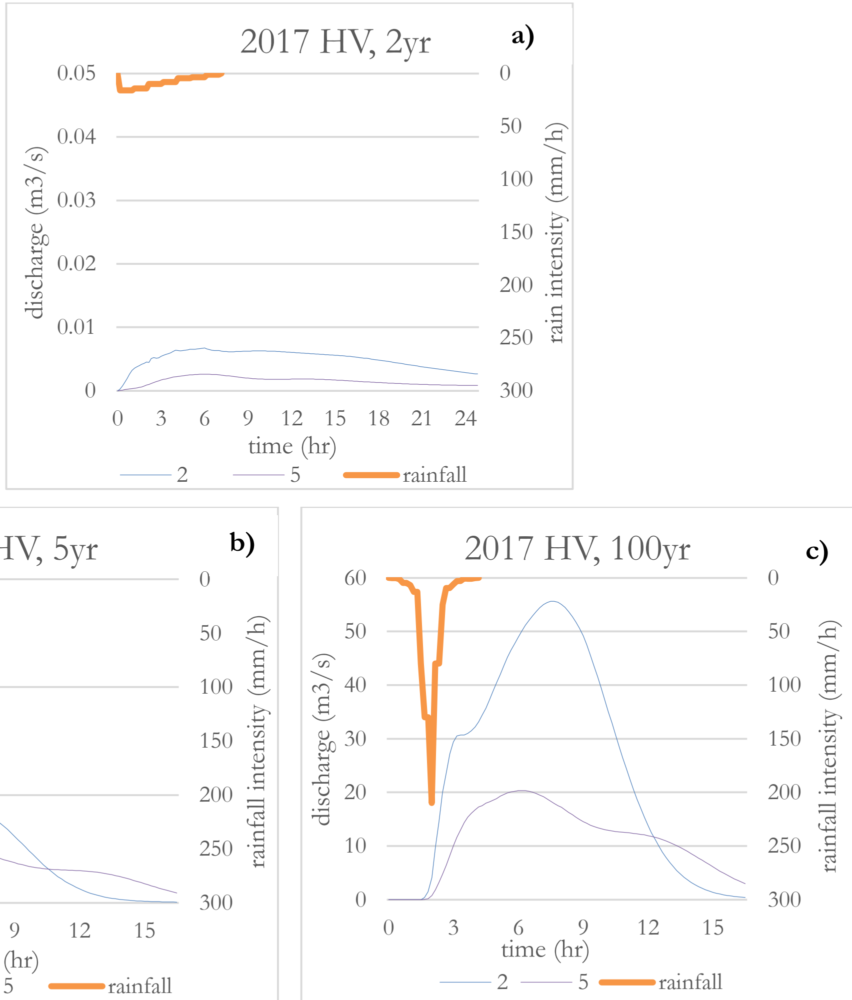

Figure 4.2 Hydrographs of rainfall with return periods of 2 (a), 5 (b) and 100 (c) year in 2017 in the wet season with high vegetation cover

4.3.3. Land cover change effect

The 5-year and 100-year return period rainstorms were used to run the LISEM model land cover maps from 2000 and 2016 on runoff discharge. The 2016 land cover map was used for scenarios of 2017. The results are shown in Table 4.11 and 4.12.

Table 4.11 Surface runoff change for a 5-year rainfall with low vegetation cover from 2000 to 2017

Low vegetation cover scenario with 5-year rainstorm	2000		2017		Percentage reduction from 2000 to 2017	
	Reservoir inlet (outlet 2)	Agricultural areas (outlet 5)	Reservoir inlet (outlet 2)	Agricultural areas (outlet 5)	Reservoir inlet (outlet 2)	Agricultural areas (outlet 5)
Peak time (hr)	6.17	7.17	6.5	7.17		
Peak discharge (m^3/s)	15.016	6.909	9.585	4.884	**36.17**	**29.31**
Total rainfall (mm)	69.277					
Total interception (mm)	1.973		2.021		**-2.43**	
Total infiltration (mm)	50.012		50.869		**-1.71**	
Total discharge (10^3 m^3)	910		818		**10.11**	
Peak discharge/ precipitation ratio (%)	19.904		17.867		**10.23**	

For a 5-year rainfall scenario, while considering the low vegetation season, the decrease in discharge is quite evident. The total discharge is reduced by 10% from **910 thousand cubic metres** in 2000 to **818 thousand cubic metres** for 16 hours 30 minutes in 2017. The peak discharge to precipitation ratio has reduced by 10% percent from **19.904** in 2000 to **17.867** in 2017. The peak discharge from outlet two has reduced by 36% from **15.016 m³/s** in 2000 to **9.585 m³/s** in 2017 while outlet 5 peak discharge has reduced by 29% from **6.909 m³/s** in 2000 to **4.884 m³/s** in 2017. Figure 4.11 shows the hydrographs.

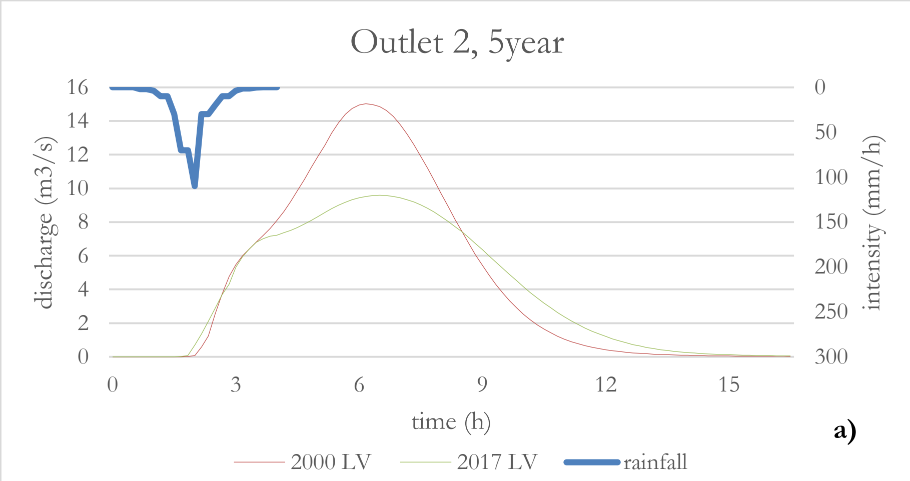

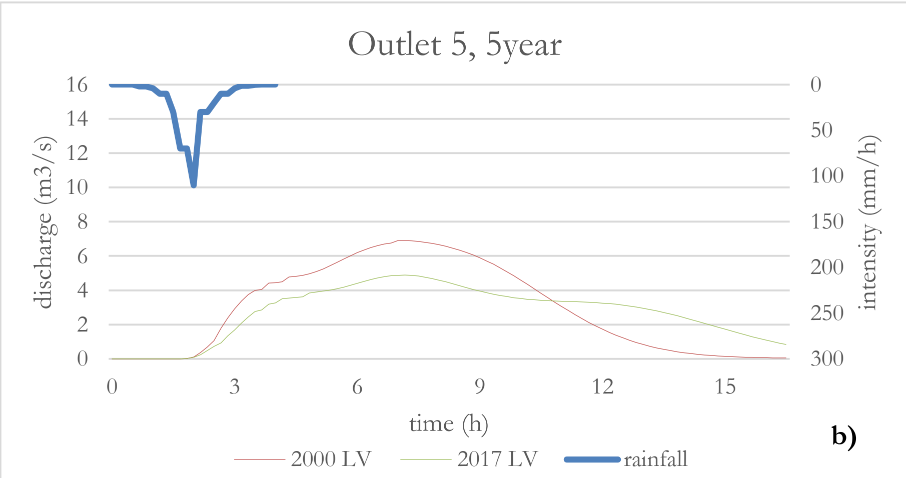

Figure 4.11 Hydrographs in the low vegetation cover season for a 5-year rainfall in 2000 and 2017 from a) the hillslopes and b) the lower slopes areas

Table 4.12 Surface runoff change for a 100-year rainfall with low vegetation cover from 2000 to 2017

Low vegetation cover scenario with 100-year rainstorm	2000		2017		Percentage reduction from 2000 to 2017	
	Reservoir inlet (outlet 2)	Agricultural areas (outlet 5)	Reservoir inlet (outlet 2)	Agricultural areas (outlet 5)	Reservoir inlet (outlet 2)	Agricultural areas (outlet 5)
Peak time (hr)	6.5	6.5	6.67	6.33		
Peak discharge (m³/s)	80.966	25.699	78.247	24.722	**3.36**	**3.80**
Total rainfall (mm)	135.433					
Total interception (mm)	1.973		2.998		**-51.95**	
Total infiltration (mm)	58.347		58.656		**-0.53**	
Total discharge (10³ m³)	4120		3940		**4.37**	
Peak discharge/ precipitation ratio (%)	46.128		44.112		**4.37**	

A 100-year return period rainfall was also used to show the effect of very high-intensity rainstorms and low vegetation cover with different land cover scenarios on surface runoff. The results are shown in Table 4.12. The total discharge from the catchment in the 2000 case was **4.120 million cubic metres** while that from 2017 dropped by 4% to **3.940 million cubic metres** in 2017. Peak discharge to precipitation ratio dropped by 4% from **46.128** in 2000 to **44.112** in 2017. There was an increase in rain interception by 50% and infiltration by about 1%. Land cover patterns influence the change in rainfall-runoff patterns in these cases with low vegetation. In the year 2000, more than 40% of the areas were bare and used for agriculture. As a result, runoff was significantly higher than in 2017 where more than 85% of the area is covered with forests as seen in Section 3.2. Figure 4.12 shows the hydrographs.

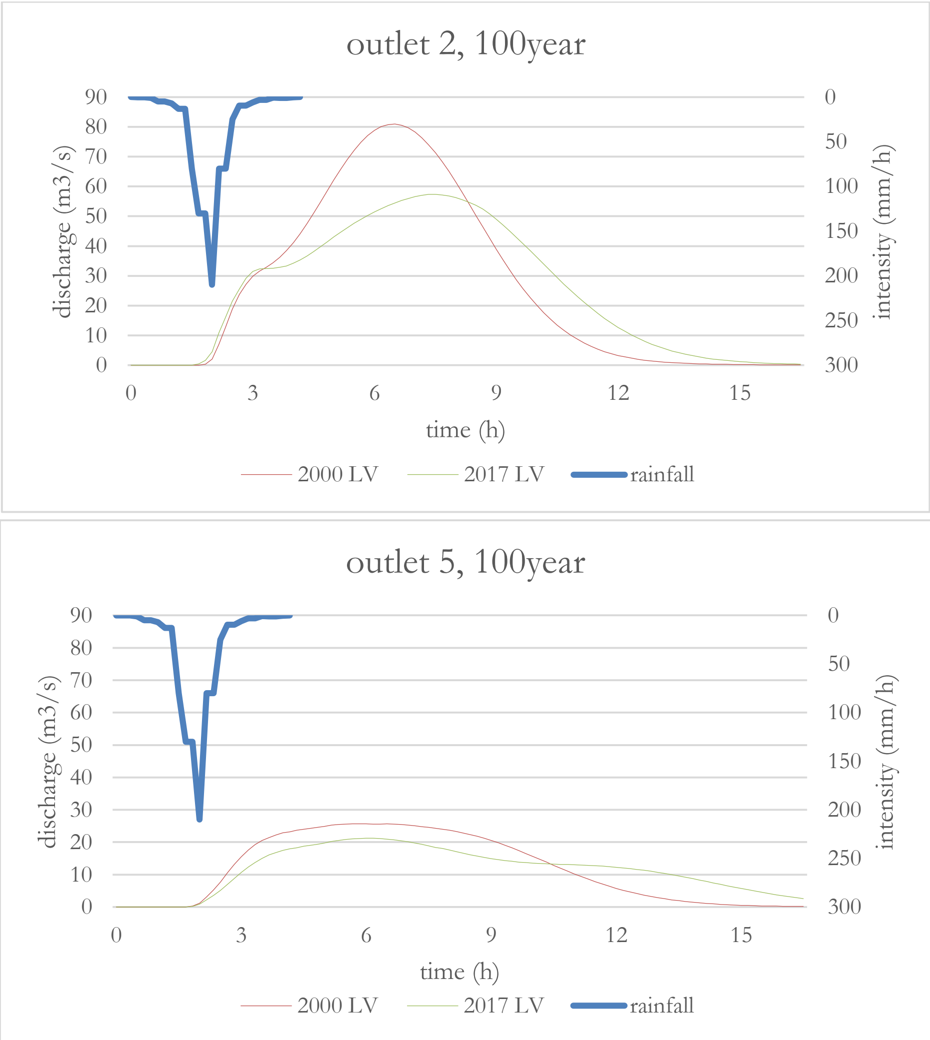

Figure 4.12 Hydrographs of 100-year rainfall in 2000 and 2017 from a) the hillslopes and b) the lower slopes areas in the low vegetation cover season

4.3.4. Vegetation cover change effect

Usually, vegetation cover is used to assess the usefulness of soil conservation techniques (Niu et al., 2014; Xu et al., 2008). Scenarios from 2000 and 2017 were combined with a high return period rainfall (100-year) to show the effect of discharge with variation in vegetation cover from the beginning of the growing season to the end (March to November) in the study area. The results are presented in Tables 4.13 and 4.14 below.

Table 4.13 Surface runoff change for a 100-year rainfall in 2000 low and high vegetation cover season

2000 Land cover with a 100-year return period rainstorm	**Low Vegetation cover**		**High Vegetation cover**		**Percentage reduction from low vegetation to high vegetation**	
	Reservoir inlet (outlet 2)	**Agricultural areas (outlet 5)**	**Reservoir inlet (outlet 2)**	**Agricultural areas (outlet 5)**	**Reservoir inlet (outlet 2)**	**Agricultural areas (outlet 5)**
Peak time (hr)	6.5	6.5	6.667	11.167		
Peak discharge (m^3/s)	80.9659	25.699	76.882	24.116	**5.04**	**6.16**
Total rainfall (mm)	135.433					
Total interception (mm)	1.973		3.599		**-82.41**	
Total infiltration (mm)	58.347		58.672		**-0.56**	
Total discharge (10^3 m^3)	4120		3912		**5.05**	
peak ratio (%)	46.128		43.791		**5.07**	

Table 4.14 Surface runoff change for a 100-year rainfall in 2017, low and high vegetation cover season

2017 Land cover with a 100-year return period rainstorm	**Low Vegetation cover**		**High Vegetation cover**		**Percentage reduction from low vegetation to high vegetation**	
	Reservoir inlet (outlet 2)	**Agricultural areas (outlet 5)**	**Reservoir inlet (outlet 2)**	**Agricultural areas (outlet 5)**	**Reservoir inlet (outlet 2)**	**Agricultural areas (outlet 5)**
Peak time (hr)	7.5	6	7.67	6.17		
Peak discharge (m^3/s)	57.334	21.210	55.607	20.338	**3.01**	**4.11**
Total rainfall (mm)	135.433					
Total interception (mm)	2.020		3.433		**-69.95**	
Total infiltration (mm)	59.651		60.019		**-0.62**	
Total discharge (10^3 m^3)	3890		3720		**4.37**	
peak ratio (%)	43.441		41.529		**4.40**	

From the results shown above, it is seen that in the event of a high-intensity rainstorm, vegetation cover reduces the impact of heavy rainfall on increased runoff discharge. With high vegetation, infiltration of water into the soil is increased. The peak ratio is also reduced in the cases of the two land cover pattern in 2000 and 2017. Interception is very significant between the low and high vegetation scenario as rain interception in the high vegetation scenario increases by 82% in 2000 and 70% in 2017 from that in the low vegetation scenario. Infiltration also increases in both cases. Vegetation cover has quite a significance on runoff discharge but largely depends on the land cover distribution. Comparing the case of 2000 with less amount of forest to that of 2017 with more forest with high vegetation cover scenarios in both case, high vegetation effect on runoff reduction will be visible when the physical properties of the dominant land cover type (forests) influences runoff distribution. The hydrographs are shown in Figure 4.13.

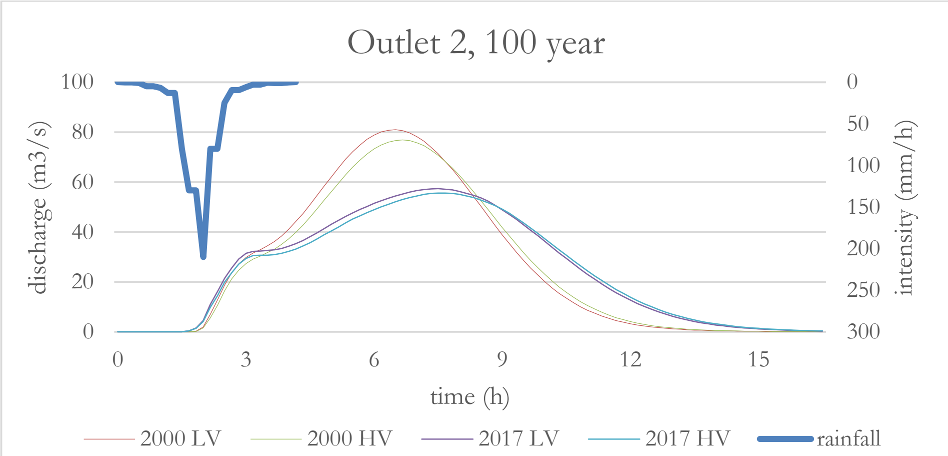

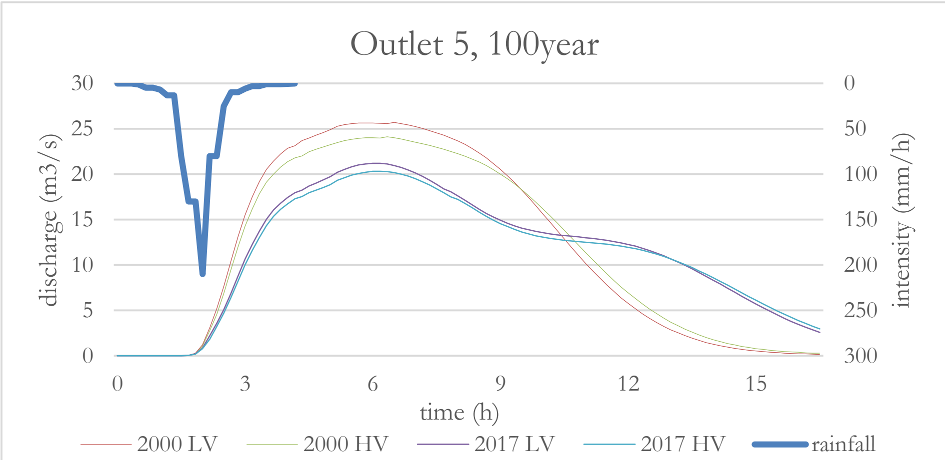

Figure 4.13 Runoff hydrographs from a) the hillslopes and b) the lower slopes areas of a 100-year rainstorm for 2000 and 2017 land cover in the dry (LV) and wet (HV) season

4.3.5. Land management and conservation

Terracing and mulching, and reforestation are land management practices carried out in the watershed. They are practised in the watershed and are shown in Figures 2.16 and 2.17. These were simulated in the model using multiplication factors as described in section 2.6. The 100-year rainfall was used as input rainfall to observe the effects of the practices in controlling runoff in cases of extreme rainfall. The model results are presented in Tables 4.15 and 4.16.

Table 4.15 Surface runoff characteristics showing the effect of terracing and mulching on agricultural fields for a 100-year rainfall

Terracing and mulching	**Peak discharge at outlet 2 (m^3/s)**			**Total discharge (10^6 m^3)**			**Peak ratio %**		
	Without	**With**	**Reduction %**	**Without**	**With**	**Reduction %**	**Without**	**With**	**Reduction %**
2000 LV	80.965	66.212	**18.2**	4.12	3.71	**10.0**	46.128	41.560	**10.0**
2017 HV	55.607	54.070	**2.8**	3.72	3.57	**4.0**	41.529	39.881	**4.0**

Table 4.16 Surface runoff characteristics showing the effect of reforestation on cropland and bare fields for a 100-year rainfall

Reforestation	Peak discharge at outlet 2 (m^3/s)			Total discharge (10^6 m^3)			Peak ratio %		
	Without	With	Reduction %	Without	With	Reduction %	Without	With	Reduction %
2000 LV	80.965	57.26	**29.28**	4.12	3.54	**14.08**	46.13	39.60	**14.15**
2017 HV	55.607	54.66	**1.71**	3.72	3.43	**7.80**	41.53	38.30	**7.78**

Table 4.15 shows the runoff characteristics when the effect of implementing terracing and mulching on agricultural fields on steeps slopes of more than 30% is simulated. When discharge measurements from the reservoir inlet (outlet 2) are considered, runoff is seen to be mostly influenced by steep slopes. The peak discharge is reduced by 18 percent when vegetation cover is at the lowest in 2000 while in 2017 with high vegetation, it is only reduced by about 2.8 percent. The total discharge from the catchment is reduced by about 10 percent for low vegetation cover scenario in 2000 while there is only a 4 percent reduction in 2017. For the whole catchment, the peak discharge to precipitation ratio is also reduced by 10 percent in 2000 while it reduces in 2017 by 4 percent. These results show that terracing and mulching in agricultural fields have a significant influence in reducing runoff. The case in 2000 is the worst case scenario in the watershed where crop fields were abundant on slopes. In 2017, quite a few of those fields have been abandoned. For the crop fields still present on those slopes, it will be a good practice to introduce terracing and mulching in those areas.

In the case of reforestation of barren and agricultural fields on hillslopes for the land cover of 2000 (Table 4.16), the hydrograph at point 2 has a peak discharge of 54.66m^3/s, a 29% reduction from that without any mitigation measures in place. There is 14% reduction in the total discharge and peak ratio by implementing reforestation in the watershed. For the present land cover (2017), there is no significant change in as the reduction in peak discharge at outlet 2 is only 1% although there is about 8% reduction in the total discharge and peak ratio. Reforestation seems to be the best practice to adopt since there is a significant reduction in runoff across the two scenarios. Reforestation efforts have increased since 2000; so that seems to be an effective strategy in reducing runoff. Therefore, there seems to be little room for further reduction shown by more reforestation measures.

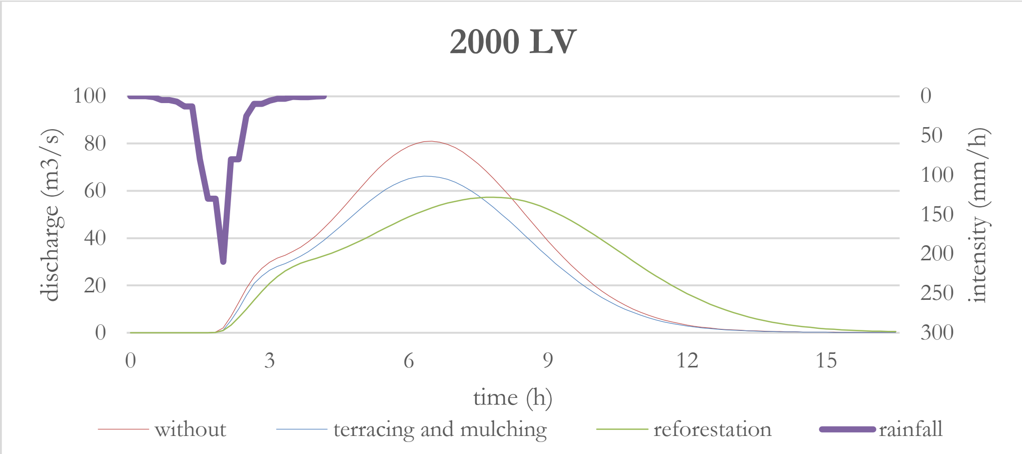

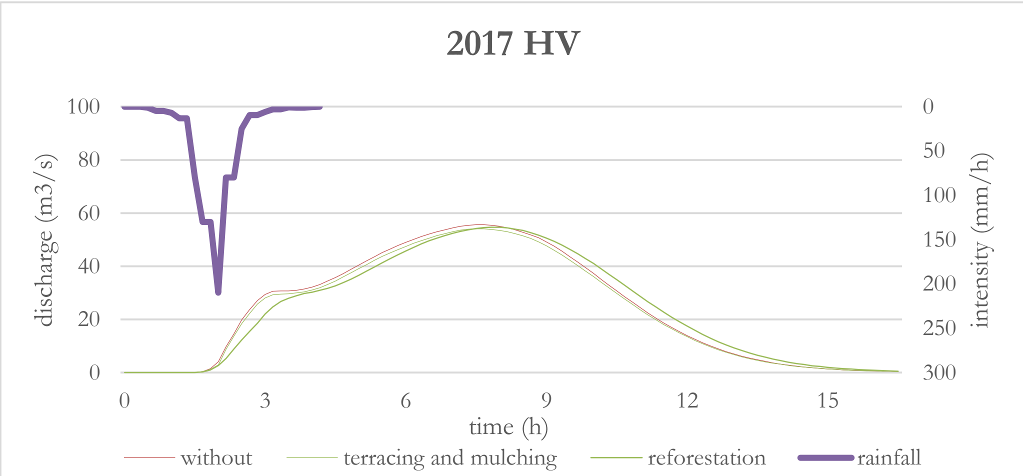

Figure 4.14 Runoff hydrographs from the reservoir inlet for a 100-year rainfall storm with effects of land management

4.4. Soil loss modelling

4.4.1. Calibration

Since validation data could not be obtained for the area, erosion data collected in 2006 was used in fitting results from the model. Soil loss rates were measured during the rainy season from May to October 2006 using experimental field plots. Eroded soil from the plots was collected using a sediment collector, dried and weighed (Shrestha & Jetten, 2018). The average erosion rates in the watershed over the six-month period are presented in Table 4.17.

Table 4.17 Field measurement of erosion rates in Nam-Chun watershed in 2006

Land cover	Average soil loss (ton/ha)
Cornfields	13 - 21
Tamarind orchards	87 - 94
Forests	2.5
Bare soil	133

While carrying out hydrological modelling using LISEM, soil loss rates were obtained by including the erosion processes at the same time as when simulating rainfall-runoff scenarios. A summary of the erosion rates for each scenario as obtained from the model are presented in Table 4.18.

Table 4.18 Soil loss rates from the LISEM model for all scenarios

Rainfall intensity return period	Land/vegetation cover scenarios	Total soil loss (ton)	Average soil loss (ton/ha)
2yr	2000 LV	15.050	0.002
	2017 LV	42.081	0.006
	2000 HV	9.158	0.001
	2017 HV	32.026	0.004
5yr	2000 LV	22,202.770	3.072
	2017 LV	14,837.141	2.049
	2000 HV	14,430.003	1.996
	2017 HV	10,173.266	1.404
100yr	2000 LV	374,840.915	51.854
	2017 LV	309,983.582	42.804
	2000 HV	301,213.902	41.669
	2017 HV	261,340.566	36.068

The values of average soil loss in Table 4.17 were used as a guide in calibrating the model to have realistic values as current erosion data for validation was unavailable. Further explanations on this results will be presented in the discussion section in Chapter five.

4.4.2. Rain intensity change effect

The effect of changes in rainfall intensity was assessed by running the model with rainstorms of different return period (2, 5 and 100-year rainstorms). Table 4.19 shows the average rates of soil loss for the dominant land cover types.

Table 4.19 Soil loss rate for rainstorms of different return periods for high vegetation season in 2017

Land cover class	Percentage of total area (%) in 2017	2017 HV 2yr soil loss (ton/ha)	2017 HV 5yr soil loss (ton/ha)	2017 HV 100yr soil loss (ton/ha)
Mixed evergreen and deciduous	**47.93**	0.793	11.755	69.845
Evergreen broadleaf	**7.20**	-0.244	-78.244	-188.228
Deciduous forest	**31.74**	0.796	20.492	83.547
Cropland	**10.55**	3.590	25.122	64.921
Barren	**0.26**	2.095	16.331	56.117

Table 4.20 Analysis of Variance (ANOVA) for rain intensity effect on soil loss

SUMMARY						
Groups	*Count*	*Sum*	*Average*	*Variance*		
2yr	3	6.4795	2.159833	1.956858		
5yr	3	57.5765	19.19217	26.38296		
100yr	3	197.734	65.91133	106.6094		
ANOVA						
Source of Variation	*SS*	*df*	*MS*	*F*	*P-value*	*F crit*
Between Groups	6537.035	2	3268.517	72.66106	**$6.23X10^{-5}$**	5.143253
Within Groups	269.8984	6	44.98306			
Total	6806.933	8				

The results were subjected to a one-way ANOVA test to statistically prove that the hypothesis that increment in rainfall intensity increases soil loss (Table 4.20). The P-value for comparing soil loss rates from 2, 5 and 100-year rainstorms from the forest, cropland and bare fields was 0.0000623 ($P<0.05$) which shows that in all land cover types, increase in rain intensity results in increased rates of soil loss. For a rainstorm with a 2-year return period with the land cover in 2017, the rates of soil loss across all types of land cover in the catchment are considerably low. Soil loss in cropland and bare areas for a rainstorm of 2-year return period is between 2.0 - 3.5 ton/ha. In the case of a 5-year rainstorm, soil loss ranges from 16 - 25 ton/ha. For a 100-year rainstorm, soil loss rates in cropland and bare 56 - 65 ton/ha. The higher soil loss rates in cropland and bare areas are as a result of the presence of lower vegetation cover than in forest areas. Soil loss due to increased rainstorm magnitude will be more significant than in forest areas. The effect of increased rainfall intensity on soil loss will be most felt in forest areas. In Table 4.19, the 100-year rainfall storm produces more substantial amounts in the forest land cover type than in the cropland or bare land cover. This observation is shown as the rainstorms with lower return periods (2-year and 5-year) have the lower soil rates from the forest land cover. For the same land cover types, increased rainfall magnitude results in higher average soil loss. For a 2-year rainstorm, soil loss is less than 1 ton/ha. In the event of a 5-year rainstorm, soil loss in forest areas ranges from 11 - 21 ton/ha while for a 100-year rainstorm, the average soil loss is between 56 - 83 ton/ha.

4.4.3. Land cover change effect

The average soil loss rates for the most dominant land cover types for 2000 and 2017 are presented in Table 4.21.

Table 4.21 Influence of land cover change on soil loss

Land cover class	Percentage of total area (%) 2000	2000 HV 2yr soil loss (ton/ha)	2000 HV 5yr soil loss (ton/ha)	2000 HV 100yr soil loss (ton/ha)	Percentage of total area (%) 2017	2017 HV 2yr soil loss (ton/ha)	2017 HV 5yr soil loss (ton/ha)	2017 HV 100yr soil loss (ton/ha)
Mixed evergreen and deciduous	**25.84**	0.782	1.693	55.831	**47.95**	0.793	11.755	69.845
Evergreen broadleaf	**1.10**	0.490	-19.926	65.967	**7.20**	-0.244	-78.244	-188.228
Deciduous forest	**42.01**	0.823	2.762	31.155	**31.76**	0.796	20.492	83.547
Cropland	**25.60**	1.739	28.699	91.350	**10.56**	3.590	25.123	64.921
Barren	**4.97**	1.078	22.219	100.176	**0.26**	2.095	16.331	56.117

Rates of soil loss across all rainfall scenarios decreased significantly with change in land cover from 2000 to 2017. In 2017, the forest areas are 85% of the total area while agricultural areas contribute about 10% of the total area. There is less than 1% of bare areas in 2017. There is an increase in soil loss from the forest types. This observation is quite unusual, but in the in evergreen broadleaf forest class, soil deposition is the dominant process which brings the overall soil loss in the forests to a minimum although the area covered by this forest type is about 7% of the total area. Soil loss from the cropland areas is reduced. Reduced soil loss rates due to a reduction in the total cropland areas in the watershed in the 2017 land cover scenario. There are fewer areas for farming on hillslopes.

4.4.4. Vegetation cover change effect

Vegetation change effect on soil loss rates was simulated using scenarios of high and low vegetation cover seasons for both 2000 and 2017. The results of rates of soil loss per land cover types are presented in Tables 4.22 and 4.23. There is a general reduction of soil loss from low vegetation cover to high vegetation cover. Statistically, to prove the hypothesis that vegetation cover is significant in controlling soil loss in the forest, cropland and barren land cover types, the results for 2017 high and low vegetation in the event of a 100-year return period rainstorm were subjected to the ANOVA test. The results are shown in Table 4.24. P-value is approximately 0.05 which means that high vegetation cover is significant in controlling soil loss for a high-intensity rainstorm.

Table 4.22 Influence of vegetation cover change on soil loss in 2000

Land cover class	Percentage of total area (%) 2000	2000 LV 2yr soil loss (ton/ha)	2000 LV 5yr soil loss (ton/ha)	2000 LV 100yr soil loss (ton/ha)	2000 HV 2yr soil loss (ton/ha)	2000 HV 5yr soil loss (ton/ha)	2000 HV 100yr soil loss (ton/ha)
Mixed evergreen and deciduous	**25.84**	0.969	-0.508	59.785	0.782	1.693	55.831
Evergreen broadleaf	**1.09**	0.660	-29.196	60.253	0.489	-19.926	65.967
Deciduous forest	**42.01**	1.047	2.186	39.637	0.823	2.762	31.155
Cropland	**25.60**	2.740	38.665	114.328	1.739	28.699	91.350
Barren	**4.97**	1.430	32.422	124.486	1.078	22.219	100.176

Table 4.23 Influence of vegetation cover change on soil loss in 2017

Land cover class	Percentage of total area (%) 2017	2017 LV 2yr soil loss (ton/ha)	2017 LV 5yr soil loss (ton/ha)	2017 LV 100yr soil loss (ton/ha)	2017 HV 2yr soil loss (ton/ha)	2017 HV 5yr soil loss (ton/ha)	2017 HV 100yr soil loss (ton/ha)
Mixed evergreen and deciduous	**47.93**	0.961	12.482	75.749	0.792	11.755	69.845
Evergreen broadleaf	**7.20**	-0.394	-95.110	-209.658	-0.244	-78.244	-188.228
Deciduous forest	**31.74**	1.157	24.709	95.792	0.796	20.492	83.547
Cropland	**10.55**	5.570	35.937	84.020	3.590	25.123	64.921
Barren	**0.26**	3.195	28.211	78.148	2.095	16.331	56.117

Table 4.24 Analysis of Variance (ANOVA) for vegetation effect on soil loss

SUMMARY						
Groups	*Count*	*Sum*	*Average*	*Variance*		
2017 LV	3	247.9385	82.64617	15.94119		
2017 HV	3	197.734	65.91133	106.6094		
ANOVA						
Source of Variation	*SS*	*df*	*MS*	*F*	*P-value*	*F crit*
Between Groups	420.082	1	420.082	6.855651	0.058903	7.708647
Within Groups	245.1011	4	61.27529			
Total	665.1831	5				

4.4.5. Land management and conservation effect

The results of simulating the effect of implementing terracing and mulching and reforestation for soil loss reduction are presented in Tables 4.25 and 4.26 respectively.

Table 4.25 Soil loss results showing the effect of terracing and mulching on agricultural fields for a 100-year rainfall storm

Terracing and mulching	Total soil loss (ton)			Average soil loss (ton/ha)		
	Without	With	Reduction %	Without	With	Reduction %
2000 LV	374,840.915	259,126.875	**30.87**	51.85	36.38	**29.84**
2017 HV	261,340.566	240,507.148	**7.97**	36.07	33.32	**7.62**

Table 4.26 Soil loss results showing the effect of reforestation for a 100-year rainfall storm

Reforestation	Total soil loss (ton)			Average soil loss (ton/ha)		
	Without	With	Reduction %	Without	With	Reduction %
2000 LV	374,840.915	256,346.225	**31.61**	51.854	35.462	**31.61**
2017 HV	261,340.566	212,156.947	**18.82**	36.07	29.28	**18.83**

For the case of terracing and mulching (results in Table 4.25), with the land cover of 2000 with low vegetation cover scenario, both the total and average rate of erosion is reduced by about 30%. In case of a land cover of 2017 with high vegetation cover, erosion rates are only reduced by about 7%. The driving cause of soil loss reduction is agricultural areas especially on slopes as is the case in the land cover of 2017. While comparing the results with that of the reforestation case (results in Table 4.26), the soil loss in 2017 is significantly reduced by about 18% as against just 7% when terracing and mulching are the only practices implemented. Reforestation of bare fields and agriculture fields on hillslopes, therefore, seems to be a lot more efficient in reducing soil loss in the catchment.

5. DISCUSSION

5.1. Expected results and implications of the study

Based on the results of the rainfall-runoff modelling, increase in forest cover was seem to have the most influence on the reduction of total amount of runoff discharge and soil loss from the catchment. However, the rates of soil loss for individual land cover types do not reflect the relationship between the increase in percentage area of forests and reduction in soil loss in individual plots. Reduction in percentage area of croplands from 25% in 2000 to 10% in 2017 have reduced runoff and soil loss from the slopes, but when the rates are compared per hectare of land, there is no significant change. When the results are compared on a smaller scale, from land cover patterns in 2000 and 2017, the runoff discharge and soil loss from 2017 became higher. The comparison infers that even when measures such as reforestation is being carried out, as shown by the increase in forests over the entire area in 2017, there needs to be specific attention given to individual land management practices on a plot-scale.

The influence of seasonal vegetation cover on runoff was also simulated in the modelling by using low and high vegetation cover situation from dry and wet seasons. It was seen that vegetation cover is essential in reducing runoff as interception of rainfall is increased. Infiltration is also increased when there is a high percentage of vegetation cover. Increased surface roughness provided by increased vegetation cover also has influenced the reduction in velocity of flow which in turn increasing infiltration. In the case of soil loss, erosion rates were seen to be dependent on the vegetation cover percentage. The lower vegetation period across all rainfall scenarios had more substantial soil loss rates than in the high vegetation cover period.

Increased rainfall intensity is the most significant factor in increasing in runoff discharge and soil loss although the influence of land cover and vegetation cover diminishes with increasing rain intensity in all scenarios. The runoff discharge and soil loss rates from the 2-year return period rainstorm for the 2017 case seem to be within the limits of the soil loss rates measured in 2006 (shown in Table 4.11). Which means there is an improvement in soil loss as the land cover distribution seem to have higher percentage forest cover. The soil loss rates presented are values collected for a 6-month period which means that different rainstorm magnitudes had influenced it. Based on the daily rainfall data from the area, there were 99 rainy days within this period. Comparing the soil loss rates for a 6-month period to the results from that of a single rainstorm as a whole may not necessarily be accurate but on the average could be comparable as a result of the effect of the accumulation of smaller rainstorms over that 6-month period.

To test the implication of land management practices in reducing runoff discharge and erosion, the land cover of 2000 with low vegetation cover was modified to have forests and terracing with mulching practices in the cropland areas on slope gradients higher than 30%. There was a significant reduction in runoff and soil loss when compared to the scenario of high vegetation and the land cover of 2017. Reforestation was seen to result in a more significant reduction of runoff than just practising terracing and mulching activities. Encouraging reforestation programs is a step in the right direction for watershed restoration. Recently, proactive efforts to control excess runoff and reduce soil loss in the area have been intensified. Those considered in section 2.2.2 were incorporated in the modelling of surface runoff and soil loss in this study. Other land management practices which are being carried out in the watershed are:

1. A dam is constructed in the middle of the watershed to control flash flooding downstream and to make water available for farmers during the dry season. The dam was constructed for controlling flood in lowland areas after the disastrous flood events of 2011. The dam is shown in Figure 5.1
2. Mixed farming: Intercropping with different types of crops with varying dates of maturity to maintain vegetation cover all year round (Figure 5.2). The presence of different plant species at various growth stages helps to reduce the velocity of flow and also helps the soil retain moisture throughout the growing season thereby increasing rain infiltration.
3. Soil loss control with Vetiver grass along slopes and river courses to retain soil in those areas and to reduce erosion (Figure 5.3). Vetiver is also used on the edges of terraces to retain the soil from slopes.

Figure 5.1 Dam for flood control

Figure 5.2 Mixed farming and mulching

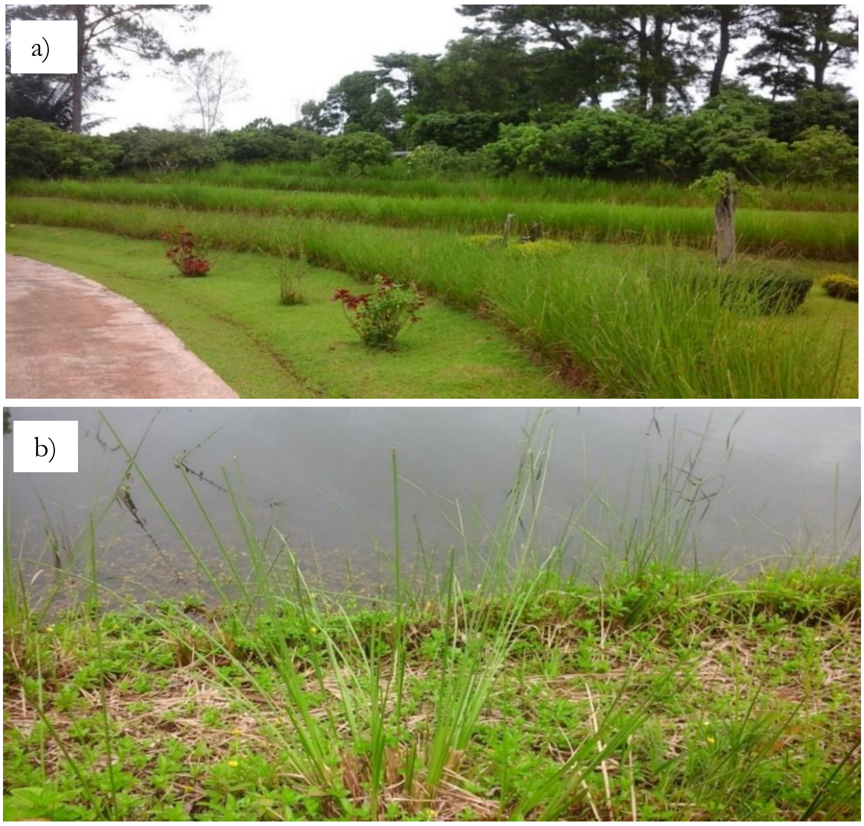

Figure 5.3 Ridging with Vetiver grass a) on a slope and b) along a stream

6. CONCLUSION AND RECOMMENDATIONS

6.1. Conclusions

For this research, remote sensing variables and field estimates of vegetation cover were used to predict vegetation cover for the whole study area as presented in section 3.2. The use of NDVI for estimating vegetation cover was improved by the use of field estimates of vegetation and field measurements of NDVI instead of using NDVI derived from remote sensing images as a proxy for indication of vegetation cover percentage for the watershed. After trying some prediction techniques, random forest regression was chosen as the means of using field point estimation to predict vegetation cover percentage for the whole watershed. It used the relationship derived from field estimates of vegetation cover from 84 locations and field measured NDVI from those locations to predict vegetation for the whole study area. The accuracy of prediction by this method was 95%.

Furthermore, evaluation of the mechanism of hydrological processes was done by creating different scenarios of vegetation to be used as input in the modelling of surface runoff and soil loss. From the results of section 4.3.4 and 4.4.4, there was a clear indication that in the dry season with low vegetation, there are higher amounts of surface runoff and soil loss from the catchment. This is because interception is reduced due to fewer leaves and less canopy cover. Infiltration is also reduced when there are fewer forest areas thereby increasing the velocity of flow, reduces surface roughness and enabling increased detachment of soil particles. Higher vegetation cover results in improved surface runoff and soil loss conditions.

As part of the methodology, three design rainstorms with 2, 5 and 100-year return periods were created and implemented in the model simulations. The 2-year return period gave the least amount of runoff while the 100-year rainstorm had the more significant amount of runoff. An analysis of variance tests was done for the three rainfall scenarios. The P value was 0.00006 ($P<0.05$) which established the fact that increasing rain intensity has a significant effect on increasing runoff and soil loss in the catchment.

Based on observations from the results of the rainfall-runoff model, areas on the hillslopes are more susceptible to generate higher runoff discharge and soil loss. This is because the velocity of water is accelerated as it flows along the hillslopes and this reduces the time of infiltration of water into the soil. The higher amount of rainfall, therefore, means that infiltration is minimal than for a lower amount of rainfall for the same duration. In the case of the scenarios implemented, the runoff discharge from a 2-year return period poses a little hazard and is lower than that for a 100-year return period rainstorm. When there is the occurrence of a higher amount of runoff discharge, there is a consequently higher amount of soil erosion.

The effects of land management were incorporated in the LISEM simulations. In terracing scenarios, slope gradient was reduced by half in areas with slopes of 30% and above. There was a 10% reduction in surface runoff discharge and 30% reduction in soil loss from the whole catchment. The reduction in both cases shows that slope gradient is a vital model parameter for runoff and soil loss modelling. The analysis of land management effects in response to increasing rainfall intensity was also carried out. From the results of the modelling of the land management scenarios with the land cover scenarios and 100-year return period rainstorm. The 100year rainstorm was the highest rainstorm return period experienced in the area as seen in the Gumbel rainfall analysis in section 4.11. Reforestation appeared to be the most efficient in overall reduction of runoff and soil loss in the catchment. Terracing and mulching practices in the agricultural areas also help in reducing runoff and soil loss. Reforestation programs are being implemented in the watershed presently. It is evident in the land cover change analysis in section 3.1, as there has been an increase in the area of forests from 2000 to 2017. This has made runoff discharge and soil loss to reduce in 2017 compared to 2000. Although this is on a large scale, efforts could be improved on a plot-scale to reduce the amount of soil loss per hectare of land.

6.2. Limitation of the research

The study encountered some limitations while carrying out rainfall-runoff and erosion modelling. Measured runoff and soil loss data for the periods considered in 2000 and 2017 were not available for proper validation of the results. Some adjustments had to be made based on general knowledge of the processes and not based on actual measurements from the study area. This imperfection resulted in some unrealistic output from the modelling. Calibration of the model was quite tricky and took much time as a result. Due to time constraints, field measurements on soil properties could not be obtained for the area where land management was practised. Adjustments were made with experimental values to simulate the effects of conservation in LISEM model in modelling the land management scenarios.

6.3. Recommendations

Some recommendations to improve the results are as follows:

1. In estimating the vegetation cover, the use of LIDAR could result in a higher accuracy of the prediction for the whole watershed. Although LIDAR data was not available in this research, the higher spatial resolution could have made estimation errors minimal.
2. The soil properties used in creating the scenarios could be improved by measurements of soil physical characteristics such as saturated hydraulic conductivity and cohesion which reflect the influence of land cover and land management on the soil properties.
3. Measured data on soil loss and discharge should be used for proper calibration and validation of and to minimise the time required for setting up the model.

REFERENCES

Artlert, K., Chaleeraktrakoon, C., & Nguyen, V. (2013). Modeling and analysis of rainfall processes in the context of climate change for Mekong, Chi, and Mun River Basins (Thailand). *Journal of Hydro-Environment Research*, *7*(1), 2–17. https://doi.org/10.1016/j.jher.2013.01.001

Barati, S., Rayegani, B., Saati, M., Sharifi, A., & Nasri, M. (2011). Comparison the accuracies of different spectral indices for estimation of vegetation cover fraction in sparse vegetated areas. *Egyptian Journal of Remote Sensing and Space Science*, *14*(1), 49–56. https://doi.org/10.1016/j.ejrs.2011.06.001

Bazrkar, M. H., Adamowski, J. F., & Eslamian, S. (2017). Water System Modelling. In J. N. Furze, K. Swing, A. K. Gupta, R. H. McClatchey, & D. M. Reynolds (Eds.), *Mathematical Advances Towards Sustainable Environmental Systems* (pp. 61–88). Cham: Springer International Publishing. https://doi.org/10.1007/978-3-319-43901-3

Belgiu, M., & Drăgut, L. (2016). Random forest in remote sensing: A review of applications and future directions. *ISPRS Journal of Photogrammetry and Remote Sensing*, *114*, 24–31. https://doi.org/10.1016/j.isprsjprs.2016.01.011

Beven, K. J. (2012). *Rainfall-runoff modelling: the primer*. https://doi.org/10.1002/9781119951001

Bidorn, B., Chanyotha, S., Kish, S. A., Donoghue, J. F., Bidorn, K., & Mama, R. (2015). The effects of Thailand's Great Flood of 2011 on river sediment discharge in the upper Chao Phraya River basin, Thailand. *International Journal of Sediment Research*, *30*(4), 328–337. https://doi.org/10.1016/j.ijsrc.2015.10.001

Blanco-Canqui, H., & Lal, R. (2010). *Principles of Soil Conservation and Management*. (Intergovernmental Panel on Climate Change, Ed.), *Climate Change 2013 - The Physical Science Basis* (Vol. 53). Dordrecht: Springer Netherlands. https://doi.org/10.1007/978-1-4020-8709-7

Breiman, L. (2001). Random forests. *Machine Learning*, *45*(1), 5–32. https://doi.org/10.1023/A:1010933404324

CNPS. (n.d.). Vegetation Program, Sampling Protocols and Projects. Retrieved 23 November 2017, from http://www.cnps.org/cnps/vegetation/protocol.php

Cuomo, S., Della Sala, M., & Novita, A. (2015). Physically based modelling of soil erosion induced by rainfall in small mountain basins. *Geomorphology*, *243*, 106–115. https://doi.org/10.1016/j.geomorph.2015.04.019

de Barros, C. A. P., Minella, J. P. G., Dalbianco, L., & Ramon, R. (2014). Description of hydrological and erosion processes determined by applying the LISEM model in a rural catchment in southern Brazil. *Journal of Soils and Sediments*, *14*(7), 1298–1310. https://doi.org/10.1007/s11368-014-0903-7

de Jong, S. M., & Jetten, V. G. (2007). Estimating spatial patterns of rainfall interception from remotely sensed vegetation indices and spectral mixture analysis. *International Journal of Geographical Information Science*, *21*(5), 529–545. https://doi.org/10.1080/13658810601064884

De Roo A.P.J., Offermans R.J.E., & Cremers N.H.D.T. (1996). LISEM: a single-event, physically based hydrological and soil erosion model for drainage basins. II: sensitivity analysis, validation and application. *Hydrological Processes*, *10*(8), 1119–1126. https://doi.org/10.1002/(SICI)1099-1085(199608)10:8<1119::AID-HYP416>3.0.CO;2-V

Fox, D. M., Witz, E., Blanc, V., Soulié, C., Penalver-Navarro, M., & Dervieux, A. (2012). A case study of land cover change (1950-2003) and runoff in a Mediterranean catchment. *Applied Geography*, *32*(2), 810–821. https://doi.org/10.1016/j.apgeog.2011.07.007

García-Ruiz, J. M., Lana-Renault, N., Beguería, S., Lasanta, T., Regüés, D., Nadal-Romero, E., … Alatorre, L. C. (2010). From plot to regional scales: Interactions of slope and catchment hydrological and geomorphic processes in the Spanish Pyrenees. *Geomorphology*, *120*(3–4), 248–257. https://doi.org/10.1016/j.geomorph.2010.03.038

Google Earth Engine. (n.d.). Retrieved 13 February 2018, from https://earthengine.google.com/

Gqd, K. S. (n.d.). STANDARD OPERATING PROCEDURE, Instructions for the Calibration and Use of a Spherical Densiometer. Retrieved from http://www.cdpr.ca.gov/docs/emon/pubs/sops/fsot00201.pdf

Grinand, C., Rakotomalala, F., Gond, V., Vaudry, R., Bernoux, M., & Vieilledent, G. (2013). Estimating deforestation in tropical humid and dry forests in Madagascar from 2000 to 2010 using multi-date Landsat satellite images and the random forests classifier. *Remote Sensing of Environment*, *139*, 68–80. https://doi.org/10.1016/j.rse.2013.07.008

Guha-Sapir, D., Hoyois, P., Wallemacq, P., & Below, R. (2016). Annual Disaster Statistical Review 2016: The Numbers and Trends. *CRED*. https://doi.org/10.1093/rof/rfs003

Hadi, Korhonen, L., Hovi, A., Rönnholm, P., & Rautiainen, M. (2016). The accuracy of large-area forest canopy cover estimation using Landsat in boreal region. *International Journal of Applied Earth Observation and Geoinformation*, *53*, 118–127. https://doi.org/10.1016/j.jag.2016.08.009

Hessel, R., & Tenge, A. (2008). A pragmatic approach to modelling soil and water conservation measures with a catchment scale erosion model. *Catena*, *74*(2), 119–126. https://doi.org/10.1016/j.catena.2008.03.018

Hölzel, H., & Diekkrüger, B. (2012). Predicting the impact of linear landscape elements on surface runoff, soil erosion, and sedimentation in the Wahnbach catchment, Germany. *Hydrological Processes*, *26*(11), 1642–1654. https://doi.org/10.1002/hyp.8282

Jensen, J. R. (2007). *Remote Sensing of Environment: an earth resource perspective* (2nd ed.). Upper Saddle River: Pearson education Prentice Hall.

Jetten, V. (2002). LISEM, 1–64.

Jetten, V. (2016). LISEM - Limburg Soil Erosion Model - User manual, 1–64. Retrieved from http://www.itc.nl/lisem/download/lisemmanualv2x.pdf

Jia, K., Liang, S., Gu, X., Baret, F., Wei, X., Wang, X., … Li, Y. (2016). Fractional vegetation cover estimation algorithm for Chinese GF-1 wide field view data. *Remote Sensing of Environment*, *177*, 184–191. https://doi.org/10.1016/j.rse.2016.02.019

Korhonen, L., Heiskanen, J., & Korpela, I. (2013). Modelling lidar-derived boreal forest canopy cover with SPOT 4 HRVIR data. *International Journal of Remote Sensing*, *34*(22), 8172–8181. https://doi.org/Doi 10.1080/01431161.2013.833361

Li, Y., Wang, H., & Li, X. B. (2015). Fractional vegetation cover estimation based on an improved selective endmember spectral mixture model. *PLoS ONE*, *10*(4), 1–15. https://doi.org/10.1371/journal.pone.0124608

Morgan, R. P. C. (2005). *Soil erosion and conservation*. Blackwell Pub. Retrieved from https://books.google.nl/books?hl=en&lr=&id=j8C8fFiPNOkC&oi=fnd&pg=PR7&dq=morgan+2009&ots=woJ5GXOeLg&sig=1quf4HQaI9EQQsgaNRL_q0YA7B0#v=onepage&q=morgan 2009&f=false

Niu, R. qing, Du, B., Wang, Y., Zhang, L. P., & Chen, T. (2014). Impact of fractional vegetation cover change on soil erosion in Miyun reservoir basin, China. *Environmental Earth Sciences*, *72*(8), 2741–2749. https://doi.org/10.1007/s12665-014-3179-8

Ouyang, W., Hao, F., Skidmore, A. K., & Toxopeus, A. G. (2010). Soil erosion and sediment yield and their relationships with vegetation cover in upper stream of the Yellow River. *Science of the Total Environment*, *409*(2), 396–403. https://doi.org/10.1016/j.scitotenv.2010.10.020

Palese, A., Ringersma, J., Baartman, J., & Peters, P. (2015). Runoff and sediment yield of tilled and spontaneous grass-covered olive groves grown on sloping land. *Soil Research*. Retrieved from http://www.publish.csiro.au/sr/SR14350

Peters, J., Baets, B. De, Verhoest, N. E. C., Samson, R., Degroeve, S., Becker, P. De, & Huybrechts, W. (2007). Random forests as a tool for ecohydrological distribution modelling. *Ecological Modelling*, *207*(2–4), 304–318. https://doi.org/10.1016/j.ecolmodel.2007.05.011

Piman, T., Pawattana, C., Vansarochana, A., Aekakkararungroj, A., & Hormwichian, R. (2016). Analysis of Historical Changes in Rainfall in Huai Luang Watershed, Thailand. *International Journal of Technology*, *7*(7), 1155. https://doi.org/10.14716/ijtech.v7i7.4709

Rahmati, M., Neyshabouri, M. R., Fakherifard, A., Oskouei, M. M., Ahmadi, A., & Sheikh, J. V. (2013). Rainfall-runoff prediction using LISEM model in Lighvan watershed, North West of Iran. *Technical Journal of Engineering and Applied Sciences ©2013 TJEAS Journal*, (2009), 1893–1901. Retrieved from www.tjeas.com

Rittima, A., Piemfa, K., Uthai, N., & Jantaramana, A. (2013). Improvement of Design Rainfall Analysis of the Central Basin of Thailand. *Engineering Research and Development*, *24*(4), 28–38.

Saxton, K. E., & Rawls, W. J. (2006). Soil Water Characteristic Estimates by Texture and Organic Matter for Hydrologic Solutions, *1578*, 1569–1578. https://doi.org/10.2136/sssaj2005.0117

SERVIR. (n.d.). Keeping watch over Forests: New Training on Forest Cover Change Detection. Retrieved 13 February 2018, from https://www.servirglobal.net/Global/Articles/Article/2549/forest-cover-change-detection-training

SERVIR-Mekong. (2015). *A Needs Assessment of Geospatial Data and Technologies in the Lower Mekong Region.*

Bangkok. Retrieved from http://servir.adpc.net/knowledge-products/needs-assessment-geospatial-data-and-technologies-lower-mekong-region

SERVIR-Mekong. (2016). Land Cover, Land Use Change and Ecosystems | SERVIR-Mekong. Retrieved 24 January 2018, from https://servir.adpc.net/service-area/land-cover-land-use-change-and-ecosystems

SERVIR-Mekong. (2017). Regional Land Cover Monitoring System Production Workshop # 3 Primitive Assembly and Accuracy Assessment Workshop.

Shrestha, D. P., & Jetten, V. G. (2018). Modelling erosion on a daily basis, an adaptation of the MMF approach. *International Journal of Applied Earth Observation and Geoinformation*, *64*(September 2017), 117–131. https://doi.org/10.1016/j.jag.2017.09.003

Shrestha, D. P., Suriyaprasit, M., & Prachansri, S. (2014a). Assessing soil erosion in inaccessible mountainous areas in the tropics : The use of land cover and topographic parameters in a case study in Thailand. *Catena*, *121*, 40–52. https://doi.org/10.1016/j.catena.2014.04.016

Shrestha, D. P., Suriyaprasit, M., & Prachansri, S. (2014b). Assessing soil erosion in inaccessible mountainous areas in the tropics: The use of land cover and topographic parameters in a case study in Thailand. *Catena*, *121*(April), 40–52. https://doi.org/10.1016/j.catena.2014.04.016

Solomon, H. (2005). *GIS based surface runoff modeling and analysis of contributing factors : a case study of Nam Chun watershed, Thailand*. University of Twente, The Netherlands. Retrieved from http://www.itc.nl/library/papers_2005/msc/ereg/harssema.pdf

Suriyaprasit, M., & Shrestha, D. P. (2007). Deriving Land Use and Canopy Cover Factor From Remote Sensing and Field Data in Inaccessible Mountainous Terrain for Use in Soil Erosion Modelling. In *The International Archives of the Photogrammetry, Remote Sensing and Spatial Information Sciences* (Vol. XXXVII, pp. 1747–1750).

United States Department of Agriculture. (n.d.). Introduction to Google Earth Engine. Retrieved from https://www.servirglobal.net/Portals/0/Documents/Articles/ChangeDetectionTraining/Module2_Intro_Google_Earth_Engine_presentation.pdf

Van der Knijff, J., Jones, R., & Montanarella, L. (1999). *Soil erosion risk assessment in Italy. Luxembourg: Office for Official Publications of the European Communities* (Vol. EUR 19022). Retrieved from http://scholar.google.com/scholar?hl=en&btnG=Search&q=intitle:Soil+Erosion+Risk+Assessment+in+Italy#0

Wang, L., Ma, B., & Wu, F. (2017). Effects of wheat stubble on runoff, infiltration, and erosion of farmland on the Loess Plateau, China, subjected to simulated rainfall. *Solid Earth*, *8*(2), 281–290. https://doi.org/10.5194/se-8-281-2017

Xu, X. L., Ma, K. M., Fu, B. J., Song, C. J., & Liu, W. (2008). Relationships between vegetation and soil and topography in a dry warm river valley, SW China. *Catena*, *75*(2), 138–145. https://doi.org/10.1016/j.catena.2008.04.016

Yen, B. C., & Chow, V. T. (1980). DESIGN HYETOGRAPHS FOR SMALL DRAINAGE

STRUCTURES. *Journal of the Hydraulics Division*, *106*(HY6). Retrieved from https://trid.trb.org/view/154722

Zafari, A., Zurita-Milla, R., & Izquierdo-Verdiguier, E. (2017). Integrating support vector machines and random forests to classify crops in time series of Worldview-2 images. *Image and Signal Processing for Remote Sensing XXIII*, 34. https://doi.org/10.1117/12.2278421

Zende, A. M., Patil, R. A., & Bhosale, G. M. (2018). Sediment Yield Estimation and Soil Conservation Measures for Agrani River Basin Using Geospatial Techniques. *Materials Today: Proceedings*, *5*(1), 550–556. https://doi.org/10.1016/j.matpr.2017.11.117

Zhou, P., Luukkanen, O., Tokola, T., & Nieminen, J. (2008). Effect of vegetation cover on soil erosion in a mountainous watershed. *CATENA*, *75*(3), 319–325. https://doi.org/10.1016/j.catena.2008.07.010

APPENDIX

Appendix 1: Google earth engine script used for vegetation cover prediction with random forest regression

```
var sept292016 = ee.Image("COPERNICUS/S2/20160929T033532_20160929T090642_T47QQU");
var sept092017 = ee.Image("COPERNICUS/S2/20170909T033529_20170909T034537_T47QQU");
var sentinel1409207 = ee.Image('COPERNICUS/S2/20170914T033531_20170914T034542_T47QQU');
var oct042017= ee.Image('COPERNICUS/S2/20171004T033601_20171004T034610_T47QQU');
var oct192017= ee.Image('COPERNICUS/S2/20171019T033729_20171019T034744_T47QQU');
var oct242017= ee.Image('COPERNICUS/S2/20171024T033821_20171024T034908_T47QQU');

// Function to mask clouds using the Sentinel-2 QA band.
function maskS2clouds(image) {
  var qa = image.select('QA60');

  // Bits 10 and 11 are clouds and cirrus, respectively.
  var cloudBitMask = Math.pow(2, 10);
  var cirrusBitMask = Math.pow(2, 11);

  // Both flags should be set to zero, indicating clear conditions.
  var mask = qa.bitwiseAnd(cloudBitMask).eq(0).and(
             qa.bitwiseAnd(cirrusBitMask).eq(0));

  // Return the masked and scaled data.
  return image.updateMask(mask).divide(10000);
}

// Map the function on the images
var composite = maskS2clouds(sentinel1409207);
var composite2 = maskS2clouds(sept292016);
var composite3 = maskS2clouds(sept092017);
var composite4 = maskS2clouds(oct042017);
var composite5 = maskS2clouds(oct192017);
var composite6 = maskS2clouds(oct242017);

//combined image, filing empty parts of 2017
var combined = composite.unmask(composite2);
//add 09092017 cloud_removed image to the 2 images in 2017
var combined_all_1 = combined.unmask(composite3);
Map.addLayer(combined_all_1, {bands: ['B8', 'B4', 'B3'], min: 0, max: 0.5},"combined_all_1");
print(combined_all_1);
//to fill masked values after cloud removal
//add 04102017
var combined_all_2 = combined_all_1.unmask(composite4);
//add 19102017
var combined_all_3 = combined_all_2.unmask(composite5);
 //add 24102017
```

```
var combined_all = combined_all_3.unmask(composite6);
Map.addLayer(combined_all, {bands: ['B8', 'B4', 'B3'], min: 0, max: 0.5},"combined_all");
print(combined_all);

//NDVI combined 3 images
var ndvi_combined_all = combined_all.normalizedDifference(["B8","B4"]);
Map.addLayer(ndvi_combined_all,{min:0,max:1,palette:["red,yellow,green"]},"nd");

//EVI
var EVI_combined_all =combined_all.expression('2.5 * ((NIR - RED) / (NIR + 6 * RED - 7.5 * BLUE + 1))',
    {'NIR': combined_all.select('B8'),'RED':combined_all.select('B4'),'BLUE': combined_all.select('B2')});
Map.addLayer(EVI_combined_all,{min:0,max:1,palette:["red,yellow,green"]},"constant");
print(EVI_combined_all);

//SR
var SR_combined_all = combined_all.expression('(NIR / RED)',{'NIR':
combined_all.select('B8'),'RED':combined_all.select('B4')});
Map.addLayer(SR_combined_all,{min:0,max:1,palette:["red,yellow,green"]},"constant");
print(SR_combined_all);

//DVI
var DVI_combined_all= combined_all.expression('(NIR - RED)',{'NIR':
combined_all.select('B8'),'RED':combined_all.select('B4')});
Map.addLayer(DVI_combined_all,{min:0,max:1,palette:["red,yellow,green"]},"constant");
print(DVI_combined_all);

var image = ee.Image(combined_all);

// Add spectral indices, NDVI and EVI
image = image.addBands(image.normalizedDifference(['B8', 'B4']).rename('NDVI'));
image = image.addBands(image.expression('2.5 * ((NIR - RED) / (NIR + 6 * RED - 7.5 * BLUE + 1))',
    {'NIR': image.select('B8'),'RED':image.select('B4'),'BLUE': image.select('B2')}).rename('EVI'));
// simple ratio SR
image = image.addBands(image.expression('(NIR / RED)',{'NIR': image.select('B8'),'RED':image.select('B4')}).rename('SR'));
//DVI
image = image.addBands(image.expression('(NIR - RED)',{'NIR': image.select('B8'),'RED':image.select('B4')}).rename('DVI'));

// Use these sentinel bands and NDVI for prediction.
var bands = ['B3','B4','B5','B6','B7','B8','B8A','NDVI','EVI','SR','DVI'];

// Load training points. The numeric property 'cover_regr' stores known labels.
var points = ee.FeatureCollection('ft:1WX_E9T5PBwq1tLGwf1DuBQAcB_ZIVvZCm2w2jfDB');
Map.addLayer(points,{palette:["red"]}, "lca_points");
print(points);
var image = image.select(bands);

// Overlay the points on the imagery to get training.
var training = image.sampleRegions(points,['cover_regr'], 1);
```

```
print("training");
print(training);

Export.table(training, "randomforest_cover_regr_trainingdata");

// Make a Random Forest classifier and train it, 10 trees.
var classifier = ee.Classifier.randomForest(10)
    .train(training, 'cover_regr',bands);

print("classifier");
print(classifier);

// Classify the input imagery.
var classified = image.classify(classifier);
print(classified);

// Get a confusion matrix representing resubstitution accuracy.
var trainAccuracy = classifier.confusionMatrix();
print('Resubstitution error matrix: ', trainAccuracy);
print('Training overall accuracy: ', trainAccuracy.accuracy());

// Sample the input with a different random seed to get validation data.
//Accuracy assessment
var trainingTesting = training.randomColumn();
var trainingSet = trainingTesting.filter(ee.Filter.lessThan('random', 0.6));
var testingSet = trainingTesting.filter(ee.Filter.greaterThanOrEquals('random', 0.6));

// Classify the validation data.
var validated = testingSet.classify(classifier);

// Get a confusion matrix representing expected accuracy.
var testAccuracy = validated.errorMatrix('cover_regr', 'classification');
print('Validation error matrix: ', testAccuracy);
print('Validation overall accuracy: ', testAccuracy.accuracy());

// Display the input and the classification.

Map.addLayer(classified, {palette: ['red','orange','yellow','green'], min: 0, max: 100}, 'classification');

Export.image(classified, "14092017randomforest_cover_regr_fullscene",
      {region: boundary_ext,crs:  'EPSG:32647',
       scale: 10});

var boundary = ee.FeatureCollection('ft:1z8Tqkybt_mjhU7TERio1evtqOfWDMmSfHslqOOuc').geometry();
Map.centerObject(boundary, 10);
Map.addLayer(boundary);
```

Appendix 2: PCRaster script used for attribute map creation (Jetten, 2002)

```
#! --matrixtable #! --lddin

binding
##################
### input maps ###
##################
DEM = demRB.map;
LU = lc2016RB.map;
SOIL = soilRB.map;
cover = vegc140917RB.map;
lutable = landuse_new.tbl;
soiltable = soil140917.tbl;

areamap
maskall.map;

initial
### LAND USE
report ch.map = lookupscalar(lutable,1,LU);
report rr.map = lookupscalar(lutable,2,LU);
report vegc.map = if(((LU eq 5) or (LU eq 11) or (LU eq 8) and (cover lt 30)), 0.9, cover/100);
report litter.map = vegc.map;
report n.map = lookupscalar(lutable,3,LU) + vegc.map*0.0055*10;
report hardsurface.map = scalar(if((LU eq 12 or road.map eq 1),1,0)); #urban areas and roads
lai = ln(1-min(vegc.map,0.99))/-0.4;
report lai.map = if(vegc.map gt 0, lai/vegc.map, 0);

#### SOIL
report coh.map = lookupscalar(soiltable,1,SOIL);
report cohadd.map = vegc.map*6;
report ksat.map = lookupscalar(soiltable,2,SOIL);
report thetas.map = lookupscalar(soiltable,3,SOIL);
report psi.map = lookupscalar(soiltable,4,SOIL);
report thetar.map = lookupscalar(soiltable,5 ,SOIL);
report thetai.map = thetar.map + 0.9 * (thetas.map - thetar.map);
report d50.map = 35 * maskall.map; # fine material (mu)
report d90.map = 120*maskall.map;
report aggrstab.map = 4 * maskall.map;

#### HYDROLOGY
report slope.map = slope(DEM);
report grad.map = sin(atan(slope(DEM)));
report ldd.map = lddcreate(maskall.map*DEM,1e31,1e31,1e31,1e31);
report accuflux.map = accuflux(ldd.map,1.0);
report streamorder.map = streamorder(ldd.map);
report channelmask.map = scalar(if(streamorder.map gt 5,1,0));
report lddchannel.map = lddcreate(if(channelmask.map eq 1,DEM),1e31,1e31,1e31,1e31);
report channelgrad.map = sin(atan(slope(if(channelmask.map eq 1,DEM))));
 ((accuflux.map/3.22e4)**1.18) );
report channeldepth.map = channelmask.map * min(5,0.2 + 0.6* ((accuflux.map/3.22e4)**1.18) );
report curvature.map = profcurv(DEM);
report channeldist.map = spread(nominal(channelmask.map),0.0,1.0);
report outlets.map = pit(ldd.map);

report channelcoh.map=100*channelmask.map;#coh.map
report chanman.map=n.map*channelmask.map;
report chanside.map= scalar(if(channelmask.map ne 0, 0));
report soildepth.map = if(grad.map gt 0.35, (1000*maskall.map), (3500*maskall.map));

smax_crop = if(LU eq 13 or LU eq 14, 0.935+(0.498*lai.map)-(0.00575*sqr(lai.map)),0);
smax_forest = if(LU eq 4 or LU eq 5 or LU eq 8 or LU eq 10 or LU eq 11,0.2858*(lai.map),0);
smax_needleleaf = if(LU eq 9, 0.2331*(lai.map),0);
smax_bare_hardsurfaces = if( LU eq 1 or LU eq 12 or LU eq 17 or LU eq 18,0.001,0);
report smax.map = smax_crop + smax_forest + smax_needleleaf + smax_bare_hardsurfaces;
```